國立臺灣大學電機資訊學院電信工程學研究所

碩士論文

Graduate Institute of Communication Engineering

College of Electrical Engineering ＆ Computer Science

National Taiwan University

Master Thesis

應用於極化分集之 61-GHz 雙饋入圓極化超大型微帶天線

61-GHz Dual-Feed Circularly Polarized Oversize Patch Antenna
for Polarization Diversity Applications

林昱宏

Yu-Hung Lin

指導教授：許博文 博士

Advisor: Powen Hsu, Ph.D.

中華民國 104 年 6 月

June, 2015

誌謝

本論文能順利完成，首先感謝許博文教授耐心的指導與栽培。許教授在學術研究上給予學生很多的空間，讓我能盡情的探索天線領域的奧妙，在遇到困難的時候，許教授總能在適當的時候給予幫助，讓研究能夠順利完成。還記得碩一剛進入老師門下，由於以前未曾接觸過天線相關知識，剛參與實驗室的 meeting，學長們的報告我完全聽不懂，老師總能藉由學長們的報告，精闢的講解出設計背後的物理意義，讓學生能快速將學長的設計與天線課程的知識做結合，在潛移默化中學會天線設計與分析的基礎能力。此外，許教授在人生哲學上有獨到的見解，以幽默詼諧的方式，闡述做人處事應有的態度，讓學生在即將邁入社會的階段，能培養正確的處事態度。

其次，感謝口試委員張知難教授、陳士元教授以及馬自莊教授，委員們的寶貴建議使論文能更臻完備。論文能順利完成，特別要感謝許派實驗室的學長們:首先感謝陳君朋學長，在碩士班兩年的生涯裡，培養我對研究及待人接物的正確態度，讓原本一竅不通的我能一窺天線的殿堂，並且在研究上面，給予我很大的幫助。感謝呂彥儒學長傳授模擬軟體的技巧，以及在每次報告完後，能精確點出研究上的問題以及提供寶貴意見。感謝吳秉勳學長在工作之餘仍從新竹來參與我的報告，分享主動電路的概念以及工作上遇到的問題，使我對微波系統以及對工作上做的事情有初步的認識。感謝曾舫剛學長、紀凱程學長、龔逸祥學長以及蔡永峰學長分享工作經驗與對天線設計的建議。

感謝季重儀先生在實作上的幫助,以及感謝台大機械工廠製作量測上的夾具，因為你們的幫助使研究更加順利。感謝電波組大家庭的學長姊同學學弟們:政豪學長、婉婷學姊、秉瑋學長、心柔學姊、振家、柏原、文譯、靜慧、怡文、承宥、子謙、依穎、碩浩、世安、呂暘、祐宸、昱敦、育琮、士竣、毅安、宏沛、秉學、蘇澤、子恆、健豪等，能跟大家一起努力一起歡笑，使我碩士生涯更加多采多姿。

最後特別感謝我的家人，因為有你們的在背後默默的支持，讓我在碩士生涯裡能全力以赴，謝謝你們。謹以此論文獻給你們。

昱宏　2015.8.11

中文摘要

　　本論文提出一種以微帶線饋入之雙圓極化之超大型微帶天線，主要操作在 61 GHz ISM 頻帶。「超大型」之概念乃是有別於傳統操作在基頻的天線，由於操作在共振頻率較高的高階模態，天線的尺寸因此被等比例放大。因為毫米波頻段的特性，設計於 61 GHz 的傳統微帶天線大小與饋入傳輸線尺寸相當，造成阻抗匹配上的困難。本論文因而提出此大型微帶天線的設計，可有效解決此問題，不須要另外設計複雜的阻抗匹配電路。除此之外，由於天線尺寸相較於操作於基頻的天線較大，在 61 GHz 因製成技術的良率及製作誤差的容忍度可得到提升。

　　論文中的天線以截角方式實現圓極化，利用兩個正交微帶線饋入，使其擁有兩相互正交的極化方向，有效應用於極化分集。由於天線的面積較大，因此不須要使用天線陣列形式，其天線增益即可大於傳統微帶天線。此外，本論文採用深入饋入方式，增加兩個輸入埠之間隔離度之頻寬。所提出的天線為簡單的單層架構。

　　藉由實作在 RO4003 板材上，以設計於 5.8 GHz ISM 頻帶來進行實驗佐證，量測結果與模擬結果相近，天線饋入埠隔離度可達 15 dB。在論文最後，未來會以此架構進行 61 GHz 之實作並量測。

關鍵字： 圓極化、高階模態、微帶天線、極化分集

ABSTRACT

In this thesis, a dual-feed dual circularly polarized oversize antenna is proposed for 61 GHz ISM band application. The term "oversize" means that comparing to conventional patch antenna operated at the fundamental mode, the proposed antenna is enlarged due to implemented at the higher-order mode. In millimeter-wave band, the dimension of the antenna is close to that of the microstrip feeding line which causes the feeding difficulties. This problem can be solved by the proposed antenna without any complicated matching networks. Moreover, since the dimension of the antenna is enlarged, the manufacturing tolerances can be increased.

The proposed circularly polarized rectangular patch antenna with is achieved by truncating its two corners. By exploiting two vertically placed microstrip feeding lines, the proposed antenna has orthogonal circular polarizations for polarization diversity applications. Owing to its enlarged size, the oversize antenna has higher gain than that of the conventional one without using array design. In addition, this design is fed by two inset microstrip lines that can enhance the isolation between the two ports. The proposed design has a simple and single-layer structure.

This design is fabricated on the RO4003 simulated and verified at the 5.8 GHz band. The simulated and measured results are in good agreement. Up to 15 dB isolation are achieved. The simulation of 61 GHz version is provided for future experimental verification.

Index Terms — circular polarizations, higher-order modes, patch antennas, polarization diversity.

CONTENTS

LIST OF FIGURES

LIST OF TABLES

Chapter 1　Introduction

1.1　Motivation

In the development of wireless communication systems, circularly polarized (CP) planar antennas have been widely investigated. Comparing to antennas with linear polarization, circularly polarized antennas have certain important advantages. The first advantage is that circularly polarized antenna is very effective in combating multi-path interferences. For instance, a RHCP antenna has a rejection of a LHCP signal which is the reflected signal. The second advantage of the circularly polarized antenna is that it is able to reduce the Faraday rotation effect that is caused by the ionosphere. That is the reason the circularly polarized antenna is widely used for signals that have gone through the ionosphere. The other advantage of circularly polarized antenna is that there is no strict direction requirement between transmitting and receiving antennas. It is different from linearly polarized antennas which are subject to polarization mismatch losses [1]. As a result, CP antennas are widely used in mobile communications, global positioning systems (GPS), wireless sensors, radio frequency identifications (RFID), wireless local area networks (WLAN), and wireless personal area networks (WPAN), and so on.

Also, since high accuracy range detection is interested in automotive and industrial applications. Thus, frequency modulated continuous wave (FMCW) radar sensors are usually used to detect the distance. Therefore, the antenna must have high gain and low profile characteristics. An example application is the fully automated production lines, where robots must be tracked to avoid collisions. This technology can be implemented in 61 GHz ISM band [2]-[5].

According to the above reasons, patch antennas with circular polarization are

suitable for millimeter wave applications due to its low profile characteristics [6]-[9]. In addition, patch antennas are often applied to polarization diversity applications. However, in millimeter-wave or sub-millimeter wave bands, conventional patch antennas are physically small that increase the difficulty of feeding and fabrication. This issue is discussed in [10]-[13].

In this thesis, an oversize dual circularly polarized patch antenna is proposed. The term "oversize" means that, unlike a conventional patch antenna that operated at the fundamental mode, the proposed antenna is operated at the higher-order mode. In other words, the length of the resonant edge is a multiple of half guided wavelengths for oversize antenna. For millimeter-wave applications, the proposed oversize antenna not only solves the feeding problems, but also increases the error tolerance of the fabrication. [14]

1.2   Literature Survey

Recently, multiple-input multiple-output (MIMO) wireless systems have been shown to have the potential for increasing the capacity in the rich multipath environments and the mitigated multipath fading. The MIMO wireless systems are based on antenna diversity technologies. One can use diversity methods to make a wireless system robust. Generally speaking, the basic principle is that signals going through several transmission channels have different fading conditions. By combining the signals from transmission paths, the fading problem can be moderated and the transmission reliability can be improved. The antenna diversities are implemented in Wireless Local Area Network (WLAN) antenna systems gradually. The major ways to classify antenna diversity are spatial diversity, pattern diversity, and polarization

diversity.

Spatial diversity employs multiple antennas that usually have similar characteristics. The space between each antenna is about several wavelengths. The separating space is chosen to maximize the received signals from one antenna when the others are at minimum. Therefore, to receive strongest signal, multiple antennas are switched in the system [15]-[17]. Pattern diversity consists of more than two co-located antennas with different radiation patterns. The radiation patterns of these antennas can cover large range of angle space [18]-[22]. Polarization diversity is an effective method to improve the reliability of WLAN systems. It consists of a pair of orthogonal polarizations (i.e. horizontal/vertical, left-had/right hand circular polarization). By using two orthogonal polarizations, the polarization mismatch losses may be reduced. Thus, the orientations of transmitting and receiving devices can be placed at random.

Among the many kinds of dual-polarized antennas, patch antennas have been used widely [23]-[42]. Patch antennas with dual linear polarization can be fed by microstrip feeding lines directly [23]-[25]. In [23] and [24], TM_{10} and TM_{01} modes of the patch antennas are excited by feeding at the center of edges. The isolation of them can achieve 20 dB with single-layer structure.

The other way to feed dual linearly polarized patch antennas is using electromagnetic coupling [26]-[31]. In [26], patch antenna with dual polarization is fed by proximity coupled quarter wave stubs. In [27], a dual-polarized antenna fed by L-probe feeding technique. The isolation is up to 30 dB. In [28], a square microstrip patch on one substrate is coupled to a pair of microstrip lines on another substrate via two orthogonal, rectangular apertures. To reduce the back radiation of slot, H-shaped coupling slots are used [29]. In [30], with modified H-shaped coupling slots, up to 34 dB isolation and 15% impedance bandwidth can be achieved. In order to improve

isolation, patch antenna is fed by two hybrid input ports; one port has two in-phase aperture-coupled feeds and the other has two-out-of-phase gap-coupled probes feed. The isolation is up to 40 dB [31]. However, multilayer antenna structures may be undesirable for many active antenna applications; a single-layer patch antenna is fed by coupled microstrip-T junctions [32].

Comparing to linear polarization diversity, only a few papers have discussed circular polarization diversity. A conventional way for circular polarization diversity is to use a dual-feed patch antenna with 90° hybrid [33]-[36]. In [37], a broadband dual circularly polarized patch is excited by four cross slots via a microstrip line with multiple matching segments underneath the ground plane. This simple design is suitable for array design. In [38], a circularly polarized patch is fed by two L-strips. The isolation between these two ports is up to 15 dB. A novel design exploits the even and odd modes in a coplanar waveguide transmission line and it enables simultaneous right- and left- handed circular polarization. More than 20 dB isolation can be achieved in a narrow bandwidth [39]. Besides, there are many reported circularly polarized antennas which are electronically reconfigurable, implemented by switching a perturbation element [40]-[42]. Since either PIN diodes or switches are required, the manufacturing costs may be increased.

1.3   Contributions

In this thesis, a dual circularly polarized patch antenna operated at higher order mode is proposed. In millimeter-wave band, the enlarged size of the antenna reduces the difficulty of the fabrication. The oversize antenna also enhances the peak realized gain. For circular polarization, the isolation between two ports can be implemented without

using switches or complicated microwave circuits. That is to say, it can simplify the difficulty of antenna design.

1.4　Chapter Outlines

This dissertation is organized as follows.

In Chapter 2, the operation principle of patch antenna is introduced. Transmission line model and cavity model for patch antenna are presented roughly. The basic theory of circular polarization and some kinds of patch antennas with circular polarization are also referred to in the final of this chapter.

In Chapter 3, the proposed dual-feed dual circularly polarized oversize antennas are presented. The concepts of isolation for circularly polarized patch antenna are mentioned. Then, the operation principle of proposed antenna is described and the limitation of impedance bandwidth is verified by changing matching transformers. The simulated and measured antenna characteristic such as S-parameters, radiation patterns, peak realized gains, radiation efficiency and axial ratio are also provided. In this chapter, this design is operated at 5.8 GHz ISM band for validation check.

In Chapter 4, the proposed dual circularly polarized oversize antenna is operated at 61 GHz ISM band. The impedance bandwidth and axial ratio bandwidth just cover this band (61~61.5 GHz). In this version, the antenna fabricated on RT/duroid 5880 substrate are simulated and analyzed.

The conclusion and future work are addressed in Chapter 5.

Chapter 2   Operation   Principles   of   Circularly

Polarized Patch Antenna

2.1   Introduction

Microstrip antennas or patch antennas are low profile, conformable to planar and nonplanar surfaces, simple and inexpensive to manufacture using modern printed-circuit technology, compatible with MMIC designs. When the particular patch shape and mode are selected, the resonant frequency, polarization, pattern, and impedance are versatile. Main disadvantages of patch antennas are their low efficiency, low power, high Q, poor polarization purity, spurious feed radiation, sensitivity to environmental factors and very narrow bandwidth.

2.2   Basic Characteristics

The geometry of microstrip antenna consists of conductive patch which is placed on the upper surface of a dielectric slab. The patch and the ground plane are separated by a dielectric sheet which is referred to the substrate. The dielectric constants are usually chosen in the range between 2.2 and 12. By exciting the proper mode beneath the patch, a conductive patch is designed that its pattern is normal to the patch.

Because better efficiency and large bandwidth are desirable for communication applications, low dielectric constant and thick substrate are good in design. However, since microstrip antennas are integrated with other microwave systems, a trade-off has to be considered between compact circuit design and good antenna performance.

The most common shapes of microstrip antennas are rectangular, square, strip and

circular since their appropriate radiation characteristics and low cross-polarization. Nonetheless, linear and circular polarization can be readily produced by one element or arrays of microstrip antenna elements.
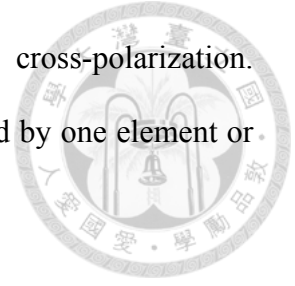
2.3 Feeding Methods [8], [9]

There are many ways to feeding patch antennas. The most common feeding method is microstrip line, coaxial probe, aperture coupling and proximity coupling.

The microstrip feed line is a conducting strip which is usually smaller than microstrip antenna connected to it. The most advantage of microstrip-line feed is easy to fabricate, simple to match by controlling the feeding position or using impedance transformer. Unfortunately, when the substrate thickness increases, surface waves and spurious feed radiation increase. As the result, the limitation of bandwidth is typical2~5%.

Coaxial-line feeds are also used widely since it is easy to fabricate. To feeding the microstrip antenna using a coaxial probe, the outer conductor is connected to the ground plane directly. The inner conductor passing through the ground plane and substrate attach to the patch. By choosing the feeding position, it is simple to matching the input impedance, and it has low spurious radiation. However, its bandwidth is as narrow as microstrip-line fed. In addition, this configuration is much more difficult to model. Both the microstrip-line feed and the coaxial-line feed inherent asymmetries that generate higher-order modes and so that it create cross-polarized radiation.

Non-contacting aperture-coupling feeds, including aperture-coupled feed and proximity-coupled feed have been brought out. An aperture-coupled feed consists of two substrates which are separated by a ground plane. A microstrip line whose energy is

coupled to the antenna through a slot on the ground plane is on the bottom side of the lower substrate. The ground plane between the substrates isolates the feed from the radiating element so as to minimize interference of spurious radiation and polarization purity. This arrangement allows the feed mechanism and the radiating element designed separately. Typically a high dielectric material is chosen as the feed mechanism, and thick low dielectric constant material as the top substrate. The matching level is decided by controlling the width of the feed line and the length of the slot. This feeding method also has narrow bandwidth and it is the most difficult fabrication of all. A similar feeding structure called proximity-coupled feed has the largest bandwidth, but its fabrication is slightly more difficult.

2.4   Rectangular Microstrip Antenna [8]

The rectangular microstrip antenna is the most popular microstrip antenna implemented by engineer. A rectangular metal patch of width W and length L is separated by a dielectric material from ground by a distance h. The two ends of the antenna can be considered as radiating edge due to fringing fields along each edge of width W. The other two edges along the sides of length L are often referred to as non-radiating edges.

Due to the finite dimension of the patch, the fields at the edges of the patch undergo fringing. The amount of fringing is related to the dimension of the patch and the height of the substrate. Therefore, it makes the patch look wider electrically compared to it physical dimension. The dimension of the patch along its length where is demonstrated in Fig. 2.1 have been extended by a distance ΔL.

The two conventional methods to analyze the rectangular microstrip antenna are

both transmission line model and cavity model which carry out CAD implementation easily. In the section of this chapter, both transmission line model and cavity model are introduced.
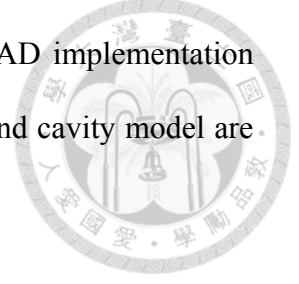
2.4.1 Transmission Line Model

The rectangular microstrip antenna consists of a microstrip transmission line with a pair of loads at either end in the transmission line model. The resistive loads at each end of the transmission line stand for radiating loss. At resonance, the imaginary part of the input impedance seen at the driving point is canceled. Thence, the input impedance turns into simple real.

For most application, the dielectric constant of representative substrate is greater than unity. The effective dielectric constant has value in the range of $1 < \epsilon_{reff} < \epsilon_r$, since some of the waves travel in the substrate and some in the air. At low frequencies, the effective dielectric constant (W/h≥1) is given as

$$W/h > 1$$

$$\epsilon_{reff} = \frac{\epsilon_r + 1}{2} + \frac{\epsilon_r - 1}{2}\left[1 + 12\frac{h}{W}\right]^{-1/2}$$

(2-1)

Since the length of the patch has extended by ΔL on each side, the effective length of the patch is larger than its physical length. For the conventional microstrip antenna, the resonant frequency is computed using

$$f_r = \frac{1}{2L_{eff}\sqrt{\epsilon_{reff}}\sqrt{\mu_0\epsilon_0}} = \frac{1}{2(L + \Delta L)\sqrt{\epsilon_{reff}}\sqrt{\mu_0\epsilon_0}}$$

(2-2)

As the substrate height increases, fringing increases and leads to larger separations

9

between two radiating edges and lower resonant frequencies.

As mention in the previous section, there are many methods to feed the microstrip antenna. Since the microstrip antenna has the maximum electric field distribution at two radiating edges, the input impedance seen at the edge is usually larger than 50 Ω. Therefore, two conventional ways to match the feeding impedance with a microstrip line are shown in Fig. 2.2 and Fig. 2.3. Fig. 2.2 is to drive the antenna at one of its radiating edges. In general, one must provide an impedance transformer to 50 Ω for this feeding method. Fig. 2.3 is to cut a narrow notch out of a radiating edge far enough into the microstrip antenna to located at 50 Ω feeding point impedance. By using this feeding method, a physical notch introduces a junction capacitance so that it influences the resonance frequency slightly.

Although the transmission line model is conceptually simple, it has some drawbacks. The transmission line model is inaccurate when used to predict the impedance bandwidth for thin substrates. Also, the transmission line model doesn't take into account the modes which are not along the linear transmission line.

2.4.2   Cavity Model

The cavity model views the rectangular microstrip antenna as an electromagnetic cavity with electric walls at the ground plane and the patch, and magnetic walls at each edge. The fields under the patch are the superposition of the resonant modes of the two dimensional radiator. The waves generated within the dielectric substrate undergo considerable reflections when arrive at the edge of the patch. The fringing of the fields along the edges of the patch is also very small whereby the electric fields is nearly normal to the surface of the patch because of the thin substrate height. Hence, only TM field configurations are considered within the cavity.

In this configuration as shown in Fig. 2.1, only a vertical electric field exists which is assumed to be constant along z-direction, in other word, only horizontal magnetic field $\overrightarrow{H_x}$ and $\overrightarrow{H_y}$ exist. Thence, the modes are described as TM_{mn} modes (m and n are integers). The integer mode index m of TM_{mn} is related to half-cycle variations of the electric field under the rectangular patch along x-axis and mode index n is related to the number of half-cycle electric field variation along y-axis. The resonant frequency for the cavity are given by

$$f_{mn} = \frac{1}{2\pi\sqrt{\mu\epsilon}}\sqrt{\left(\frac{m\pi}{L}\right)^2 + \left(\frac{n\pi}{W}\right)^2} \qquad (2\text{-}3)$$

The mode with the lowest order resonant frequency is referred to as the dominant mode (fundamental mode). For all microstrip antennas $h \ll L$ and $h \ll W$. If $L > W$, the mode with the dominant mode is the TM_{10} modes whose resonant frequency is given by
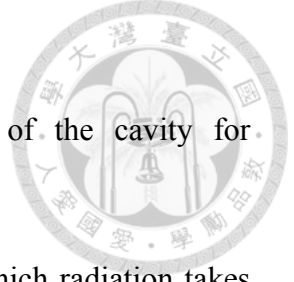
$$f_{10} = \frac{1}{2L\sqrt{\mu\epsilon}} = \frac{v_0}{2L\sqrt{\epsilon_r}} \qquad (2\text{-}4)$$

where v_0 is the speed of light in free-space. In addition, if $L > W > L/2 > h$, the second order mode is the TM_{01} whose resonant frequency is given by

$$f_{01} = \frac{1}{2W\sqrt{\mu\epsilon}} = \frac{v_0}{2W\sqrt{\epsilon_r}} \qquad (2\text{-}5)$$

However, if $L > L/2 > W > h$, the second order mode is the TM_{20}, whose resonant frequency is given by

$$f_{20} = \frac{1}{L\sqrt{\mu\epsilon}} = \frac{v_0}{L\sqrt{\epsilon_r}} \qquad (2\text{-}6)$$

11

The tangential electric field distribution along the side walls of the cavity for the TM_{10}, TM_{01}, TM_{20}, TM_{02}, is a shown in Fig. 2.4 respectively.

The four sidewalls represent four narrow apertures through which radiation takes place. From Huygen's Principle, the equivalent magnetic current density is

$$M_s = -\hat{n} \times E_a \qquad (2\text{-}7)$$

where E_s represents the electric fields at the slot.

Using the transmission line model, there are a total of four slots representing the microstrip antenna, only two accounts for most of the radiation. The other two slot separated by the width W of the patch, cancel along the principle planes. In order for the fields at the aperture of the two slots to have opposite polarization, the slots are separated by a transmission line of length L, which is approximately $\lambda_g/2$. The equivalent magnetic current densities along the two slots, each of width W and height h, are both of the same magnetic and of the same phase. These two sources referred as radiating slots add in a direction normal to the patch and ground plane forming a broadside pattern. On the other hand, the current densities on the other wall are of the same magnitude but of opposite direction, which let the fields radiate by these two slots cancel each other in the principle H-plane. Since corresponding slots on opposite wall are $180°$ out of phase, the corresponding radiations cancel each other in the principle E-plane. Therefore, these two slots are referred to as non-radiating slots.

2.5   Circular Polarization [8], [9], [42]

Polarization of an antenna is related to the orientation of electric fields radiated by

the antenna. To produce circular polarization, two orthogonal components of electric fields in the far field region are required. The electrical field radiated by an antenna can be written as

$$\vec{E}(\theta, \varphi) = \vec{\theta}E_\theta(\theta, \varphi)e^{j\emptyset_1} + \vec{\varphi}E_\varphi(\theta, \varphi)e^{j\emptyset_2} \tag{2-8}$$

$E_\theta(\theta, \varphi)$ and $E_\varphi(\theta, \varphi)$ are two magnetics of electric field components in the far filed. $\emptyset_1$ and $\emptyset_2$ are the phase shift of each electric field component.

If the total electric field has two orthogonal components which have the same magnitudes and a 90° phase difference between the two component, represented by

$$E_\theta(\theta, \varphi) = E_\varphi(\theta, \varphi)$$

$$\emptyset_1 - \emptyset_2 = \pm\frac{\pi}{2} \tag{2-9}$$

In reality, it is difficult to achieve a prefect circular polarization, hence the curve traced at a given position as a function of time which is usually an ellipse. The ratio of the major axis and the minor axis of the ellipse is known as axial ratio (AR). Usually, axial ratio is required to be below 3dB for a circularly polarized antenna.

2.5.1 Double-Feed Circularly Polarized Rectangular Microstrip Antenna

Fig. 2.5 shows a rectangular microstrip antenna fed by 90° branch line hybrid which creates circular polarization. The TM_{01} and TM_{10} which have the same resonant frequency are orthogonal. These excited modes fed by the branch line hybrid have equal amplitude and 90° phase difference at the hybrid's center frequency to produce circular polarization. With this two feeding point arrangement, each probe is always positioned at a point where the field generated by the other probe exhibits a null,

therefore, there is little mutual coupling between the two probe.

The other conventional method is achieved by the difference in the line lengths to the patch feeds such as power divider as shown in Fig. 2.6.

The disadvantage of the branch line hybrid and power divider is that the impedance mismatch causes power rejection and destroys good circular polarization. In addition, the reflections that couple to the splitter output ports result in radiation of the opposite hand of polarization.

2.5.2 Single-Feed Circularly Polarized Rectangular Microstrip Antenna

The common methods used to create circularly polarized radiation from a rectangular microstrip antenna with a single driving point illustrated as follow.

Fig. 2.7 shows the nearly square patch whose dimension L and W are nearly the same so that the resonant frequencies of the TM_{10} and TM_{01} overlap significantly. Both of their magnitudes are identical and their phases are different to 90°.

The second method in Fig. 2.8 is to place a diagonal slot across the patch. The dimension of the slot can produce circular polarization. It is necessary to keep the slot narrow so that the secondary slot radiator does not be created.

The third method in Fig. 2.9 illustrates the square microstrip antenna with a pair of truncated corners. This creates a pair of diagonal modes that are no longer TM_{10} and TM_{01} as the shape of the patch changed. If the pair of corners is reduced, the capacitance along that diagonal reduces, making it more inductive. The amount of the area removed can be adjusted so the phase of the truncated corner diagonal is 45° and the unmodified diagonal is −45°. The polarization sense is reversed by reversing the position of the corners.
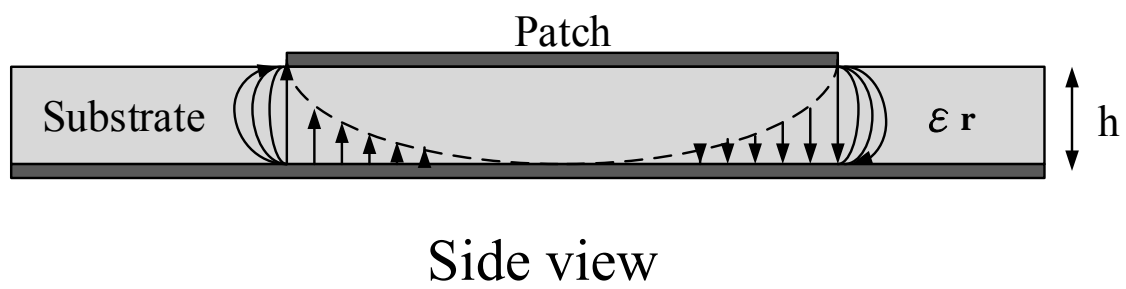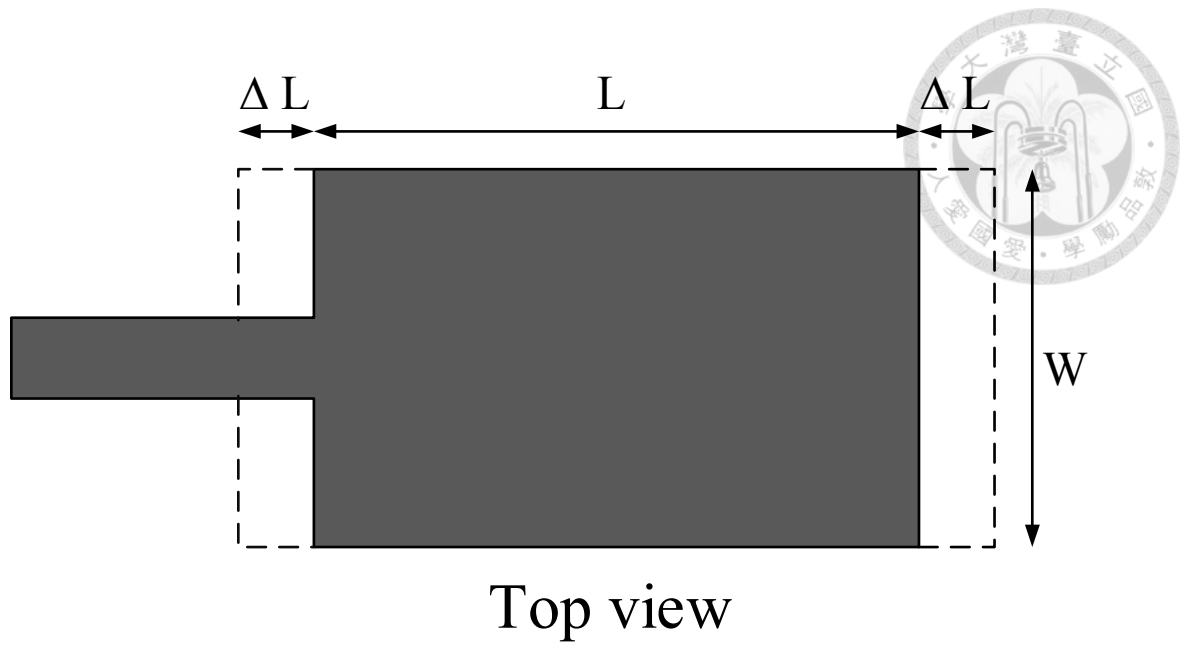
Top view

Side view

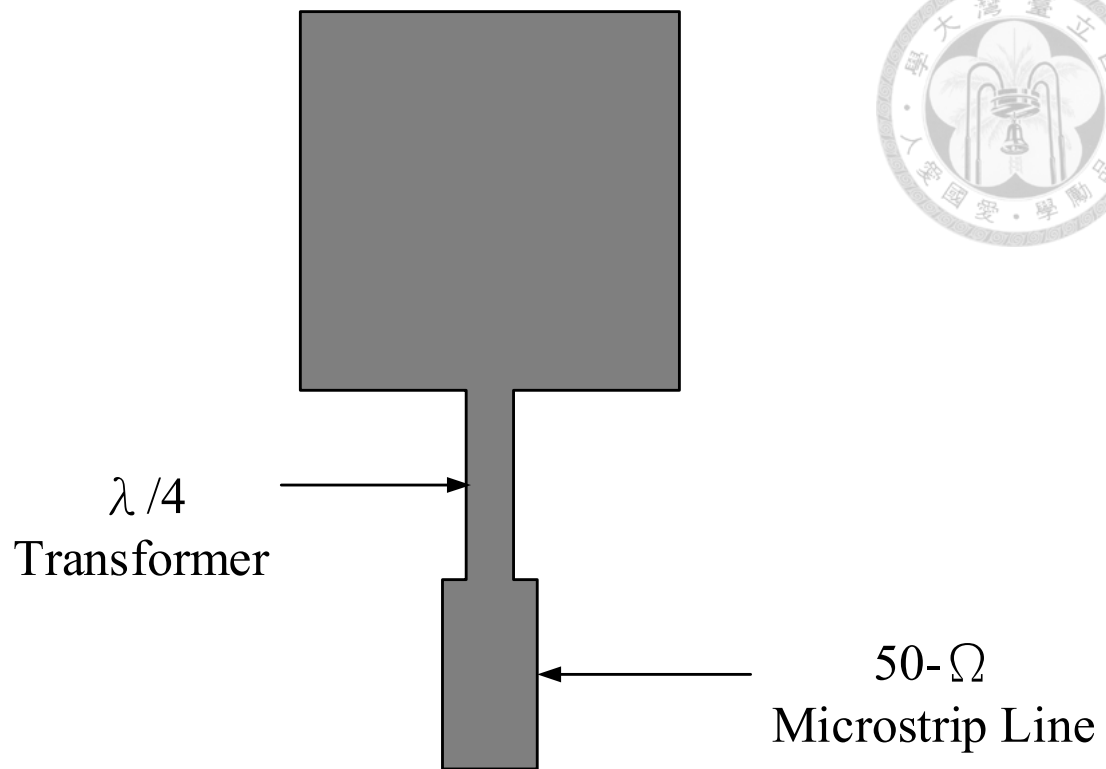Fig. 2.1 A typical rectangular microstrip antenna

$\lambda /4$
Transformer

50-Ω
Microstrip Line

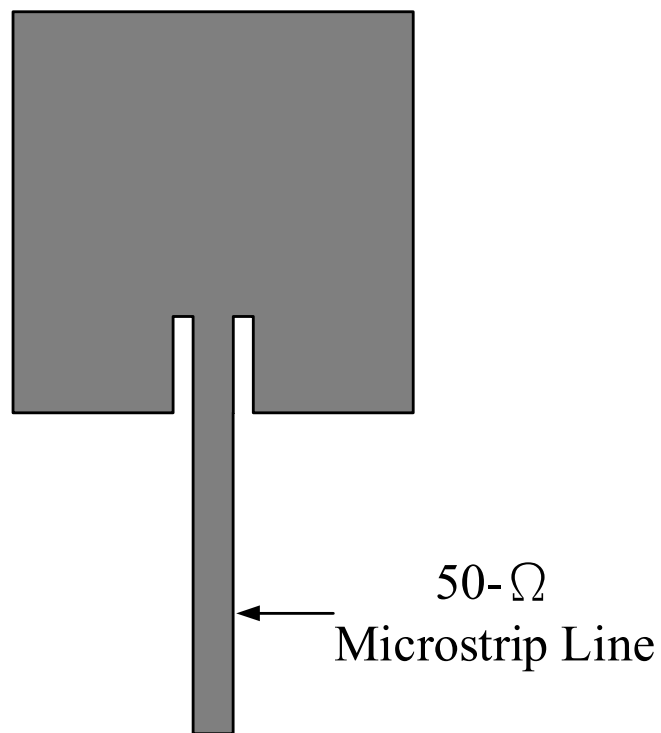Fig. 2.2 Microstrip-line feed at its edge
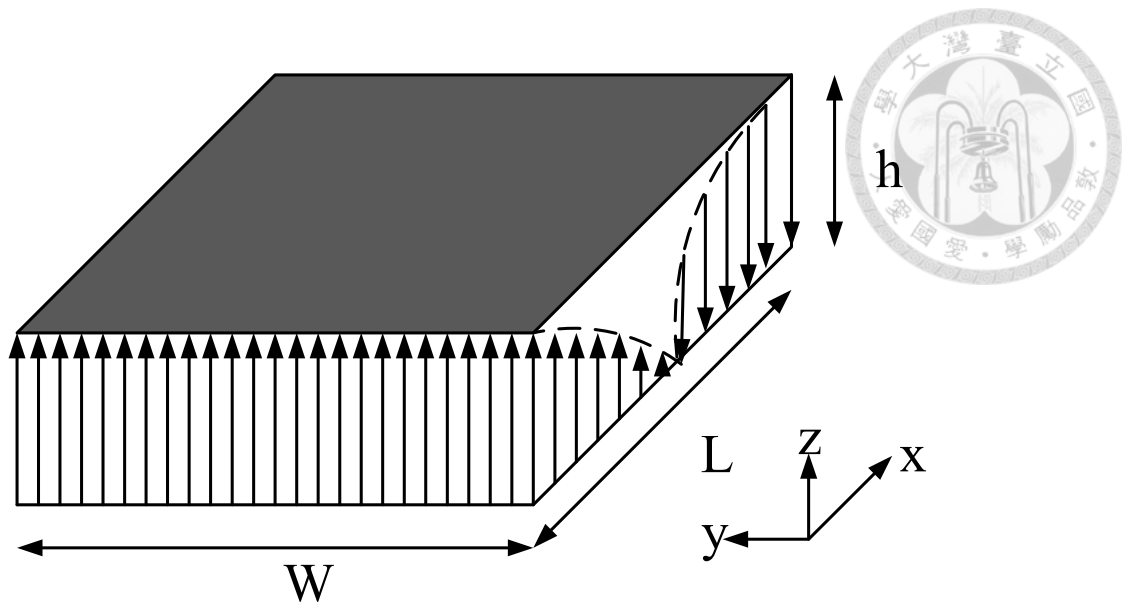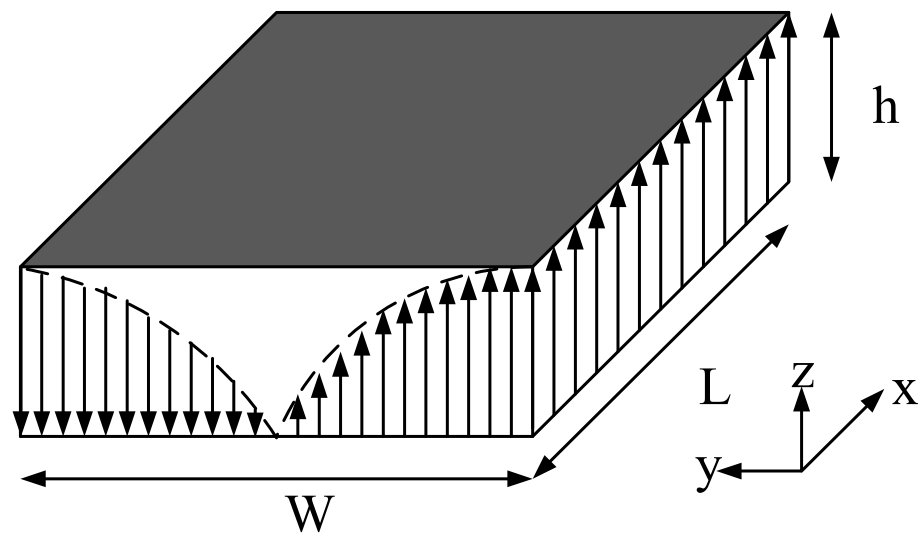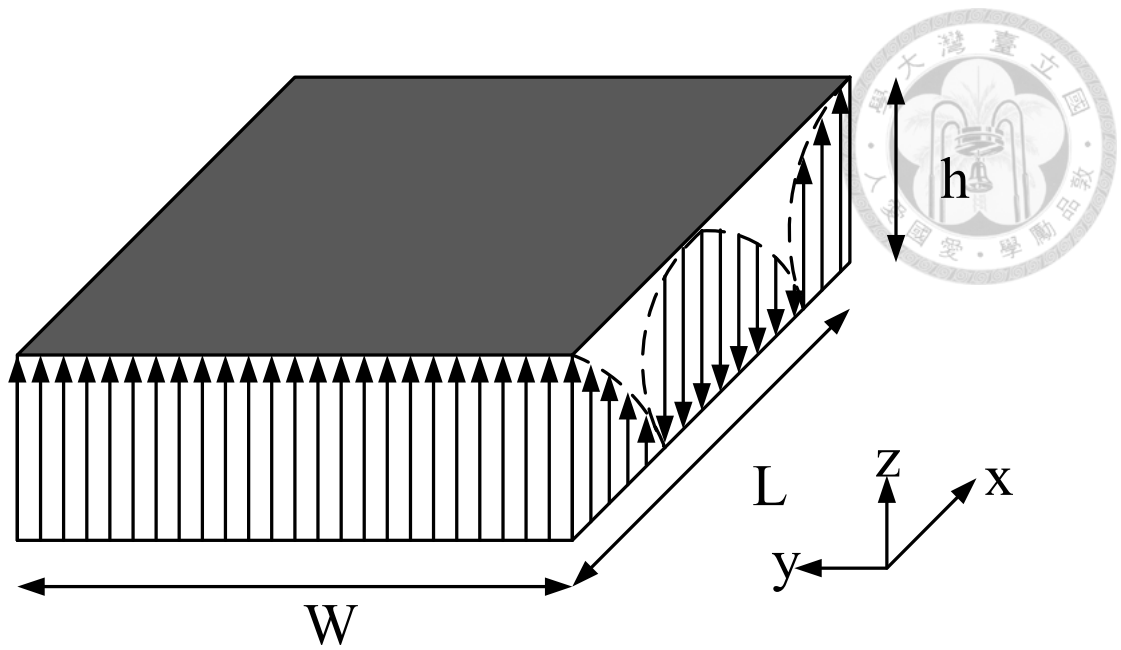

50-Ω
Microstrip Line

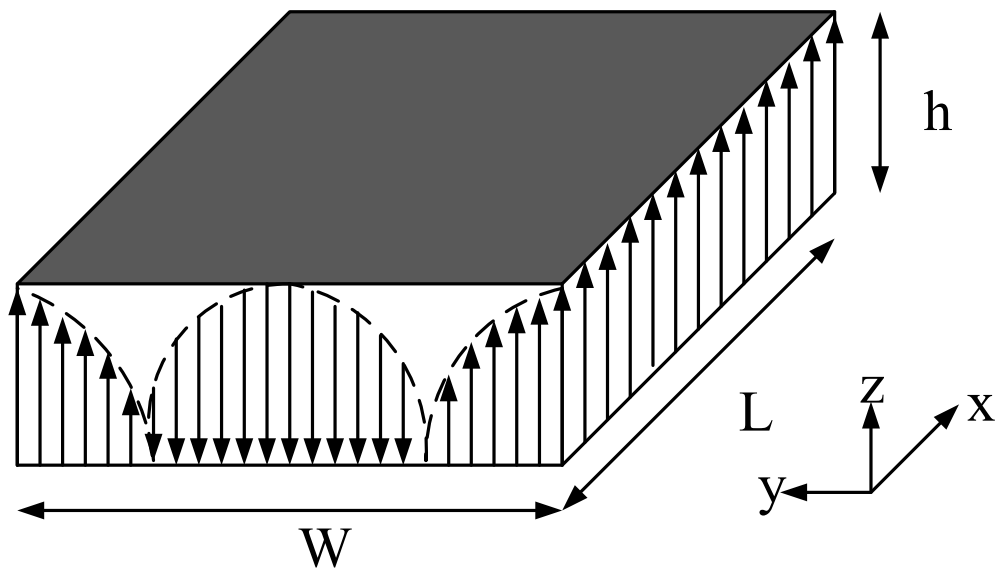Fig. 2.3 Recessed microstrip-line feed

(a) TM_{10} mode

(b) TM_{01} mode

(c) TM$_{20}$ mode

(d) TM$_{02}$ mode

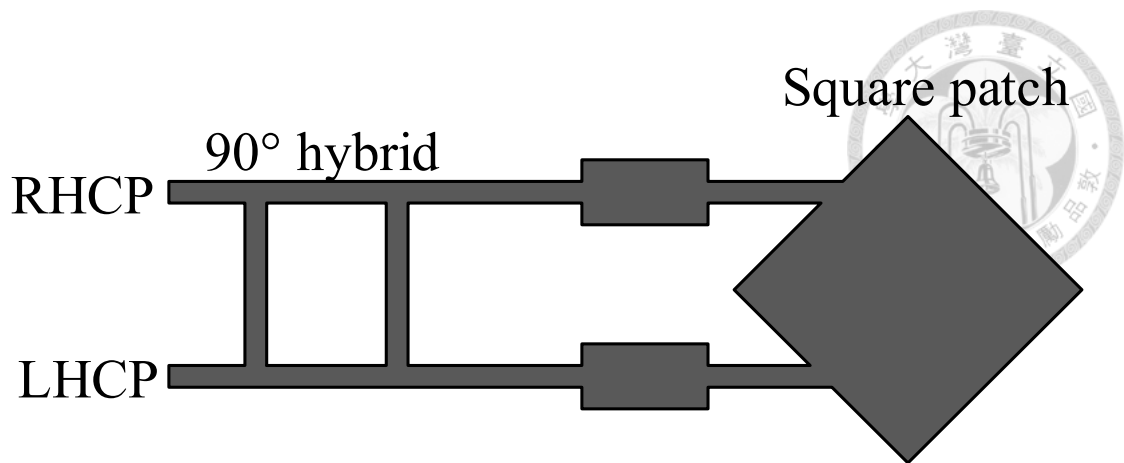Fig. 2.4 Field configurations in rectangular microstrip antenna
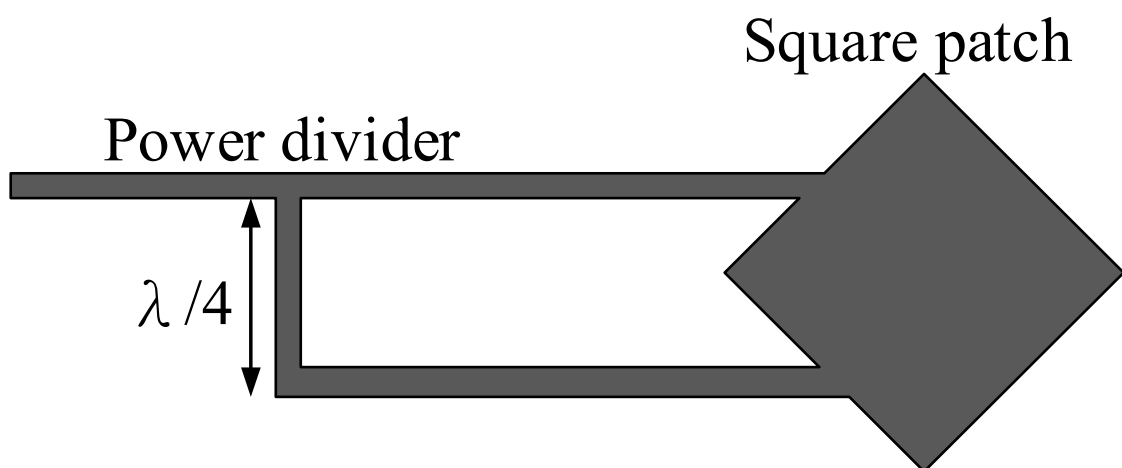
Fig. 2.5 Square patch driven by 90° branch line hybrid
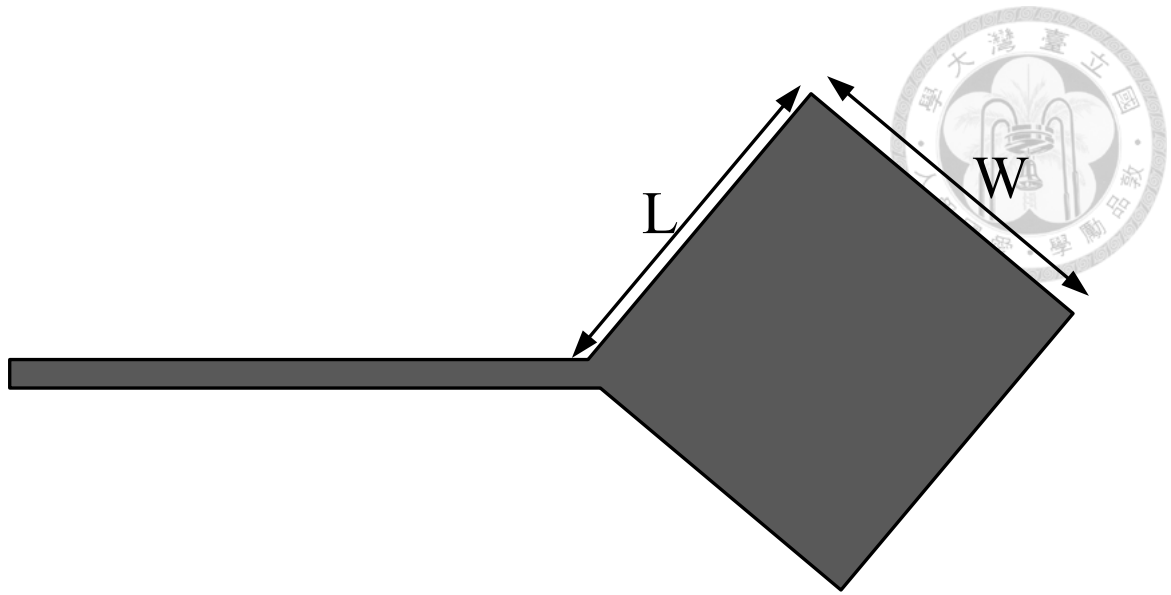

Fig. 2.6 Square patch driven by power divider

Fig. 2.7 Nearly square microstrip antenna
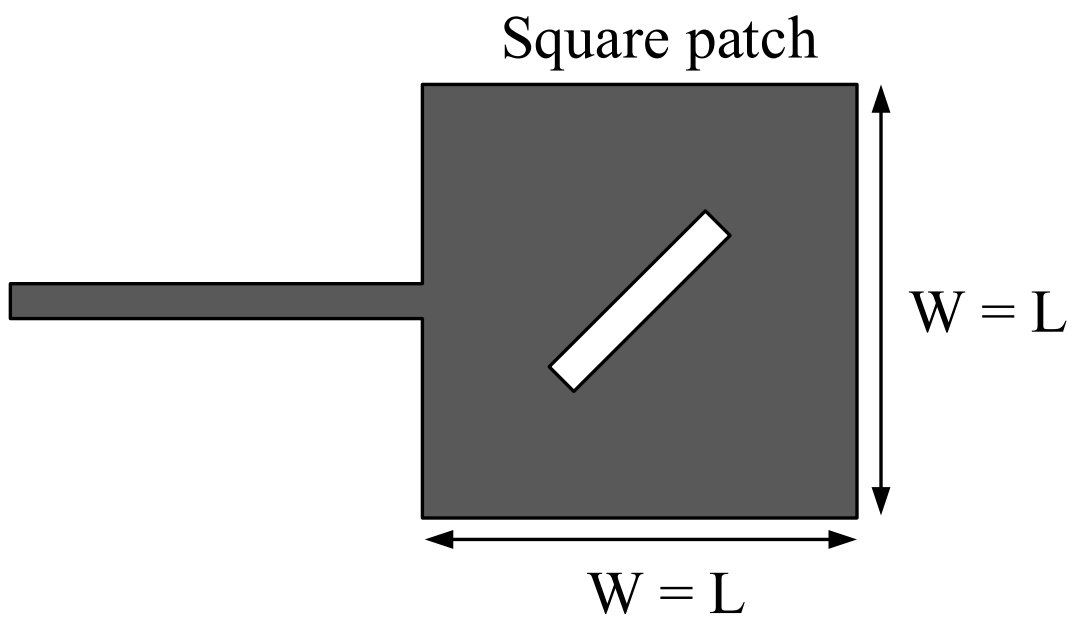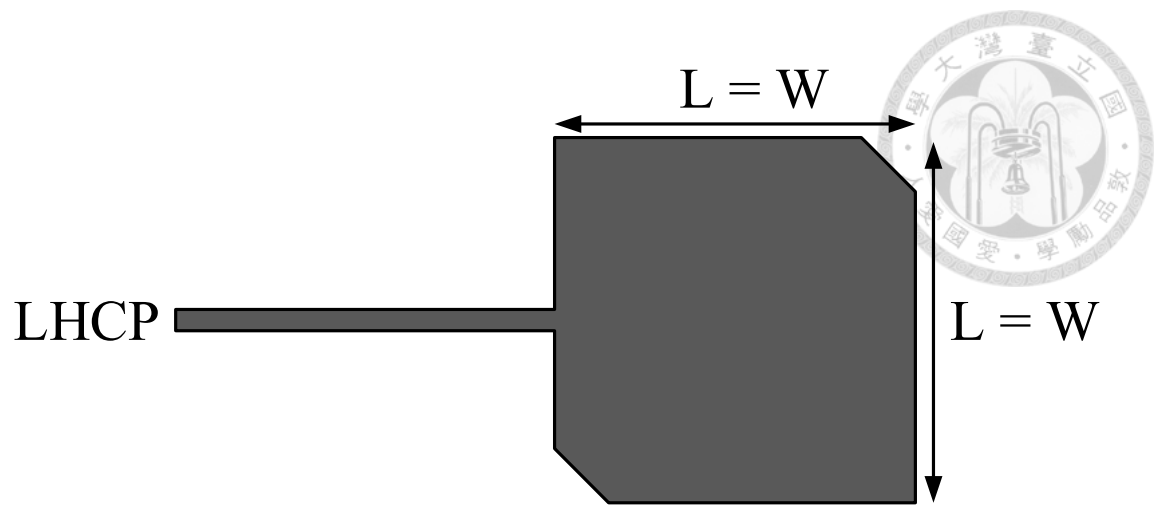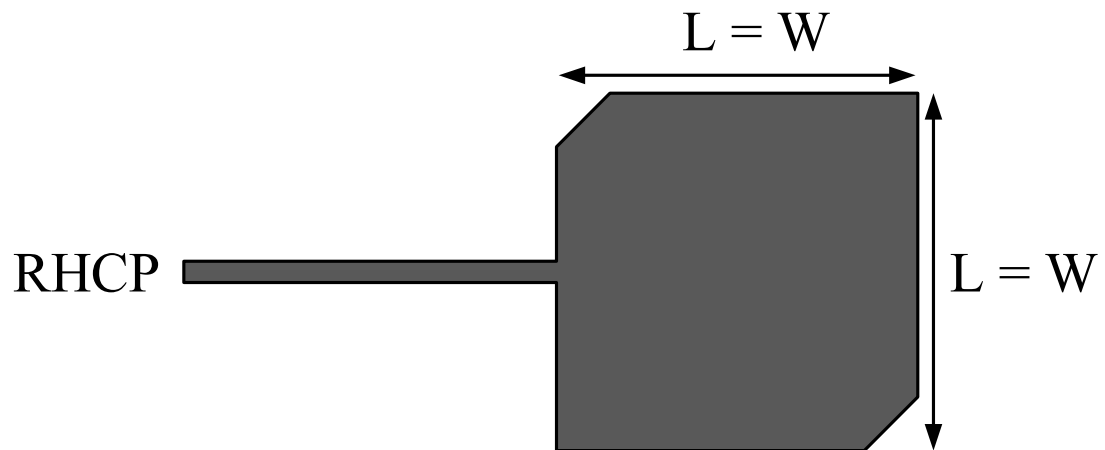
Square patch

W = L

W = L

Fig. 2.8 Square patch with thin slot for circular polarization

(a) Left-hand circular polarization (LHCP)

(b) Right-hand circular polarization (RHCP)

Fig. 2.9 Circular polarization by truncating opposite corners of square patch

Chapter 3 Dual-Feed Oversize Patch Antenna with Dual Circularly Polarization at 5.8 GHz ISM band

As mentioned in previous Section, the size of millimeter wave antennas operated at fundamental mode lead to low tolerance of fabrication error and feeding problems. In order to solve above problems, a circularly polarized oversize microstrip antenna operated at TM_{30} mode is presented in this chapter. Although there are many other higher order modes in a microstrip antenna, the TM_{30} mode is chosen owing to its broadside radiation. By using higher-order modes, the antenna gain is higher than conventional microstrip antenna without using array forms. The geometry of circularly polarized patch antenna operating at TM_{10} and TM_{30} mode are shown in Fig. 3.1. It is obvious that the area of oversize antenna is nine times as big as conventional one. Comparing to the directivity of oversize and conventional antenna, both directivity of antenna at 5.8 GHz are shown in Fig. 3.2. From Fig. 3.2, the directivity of conventional antenna is about 7 dBic. However, the oversize antenna is more than 11 dBic at center frequency.

This higher-order mode antenna is designed at 5.8 GHz in this chapter for a validation check. A 61 GHz ISM band version is presented in the next chapter.

3.1 Isolation Design

3.1.1 Concepts of Isolation for circularly polarized patch antenna

In the previous Chapter, the mode distributions of rectangular patch antenna are mentioned. The patch antenna can be modeled by a dielectric-load cavity with two perfectly conducting electric walls and four perfectly conducting magnetic walls. From boundary condition, tangential electric field must be zero so that the electric field lines are perpendicular to the upper patch and lower ground. Also, a typical electric field lines for microstrip line are shown in Fig. 3.3. Most of the electric field lines concentrate in the substrate and are almost perpendicular to microstrip line and ground.

In general, the coupling coefficient of coupled RF/microwave resonators, which can be different in structure and can have different self-resonant frequencies, may be defined on the basis of a ratio of coupled to stored energy, i.e.

$$
k = \frac{\iiint \epsilon \vec{E}_1 \cdot \vec{E}_2 dv}{\sqrt{\iiint \epsilon |\vec{E}_1|^2 dv \times \iiint \epsilon |\vec{E}_2|^2 dv}} + \frac{\iiint \mu \vec{H}_1 \cdot \vec{H}_2 dv}{\sqrt{\iiint \mu |\vec{H}_1|^2 dv \times \iiint \mu |\vec{H}_2|^2 dv}} \tag{3-1}
$$

where $\vec{E}$ and $\vec{H}$ represent the electric and magnetic field vectors and k represents the coupling coefficient shown in Fig. 3.4. The first term on right-hand side represents the electric coupling, while the second terms represents the magnetic coupling. The interaction of the coupled resonators is mathematically described by the dot operation of their space vector fields. A positive sign would imply that the coupling enhances the stored energy of uncoupled resonators, whereas a negative sign would indicate a reduction [43].

The distribution of electric field in microstrip line is nearly parallel to electric field in the microstrip antenna. Also, the coupling coefficient may have maximum absolute value because of the dot operation. As a result, if the feeding positions are not chosen appropriately, the energy excited by one port goes through the microstrip patch to another port and gets poor isolation between two feeding line. In order to obtain good isolation, the feeding points are placed on the electric field null position of the microstrip antenna.

For a conventional circularly polarized square patch with truncated corner operated at fundamental mode, the electric field null position of two orthogonal modes is at the point of intersection as shown in Fig. 3.5; that is to say, the electric field null position is at the center of patch. Hence, it is difficult to have good isolation between two ports. However, when a patch antenna operate at higher-order modes, there exists more than one electric field null positions in the patch. The actual electric field null positions depend on the substrate and the truncated corner size. By finding the null positions of electric field, good isolation can be implemented. Therefore, the circularly polarized patch antenna operating at TM_{30} mode not only increases the manufacturing error tolerance of fabrication but also enhances the isolation between two ports.

3.1.2 Design Procedure

Based on the simplified formulation that has been described, a design procedure for dual circularly polarized patch antenna is shown as follows,

1. Select substrate material, substrate thickness, and operating frequency.

2. Determine the effective dielectric constant of the patch antenna using equation (2-1).

3. Choose the operating mode of patch antenna by using equation (2-3).

4. For rectangular patch, the edge L is equal to W, which leads to TM_{m0} and TM_{0n} mode operating at the same frequency.

5. Truncate the diagonal corners of patch antenna so that the circular polarization can be generated.

6. Find the electric field null position of microstrip patch by recessed microstrip-line feed.

7. If the input impedance is not $50\ \Omega$, an impedance transformer is used to match the feeding point.
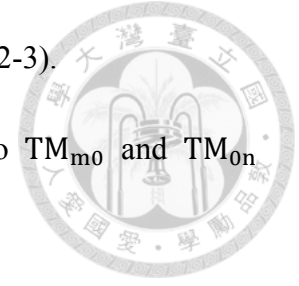
3.2   An Dual-Feed Dual Circularly Polarized Oversize Patch Antenna with Quarter Wave Transformer

3.2.1   Antenna Design and Analysis

The geometry of the proposed antenna is shown in Fig. 3.6. This square patch antenna with truncated corner is fed by two perpendicular microstrip lines directly exciting right-hand circular polarization and left-hand circular polarization at near 5.8 GHz. To enhance the isolation between two feeding points, the inset feeds are applied to find the null position of the electric field. The inset feeds affect the current distribution on the patch slightly, but the isolation between two ports is extremely enhanced. It is a trade-off between axial ratio and isolation. By doing so, the unwanted coupled energy is reduced greatly.

The simulated distribution of current on the microstrip patch is shown in Fig. 3.7. For the square patch, the current forms 1.5 λ_g distribution along edges.
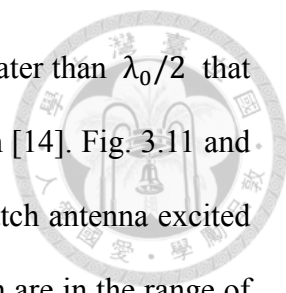
3.2.2   Simulation and Measurement Results

The proposed antenna is implemented and tested. The dielectric substrate is the RO4003C with the dielectric constant $\epsilon_r = 3.55$, loss tangent $\tan\delta = 0.0027$ and thickness $h = 1.524$ mm. The ground plane dimension is 70×70 mm^2. The feeding microstrip lines are designed to match the 50Ω SMA connectors. All simulations were gone through by software HFSS during this design procedure. All design parameters are listed in Table 3.1.

The simulated and measured S-parameters are shown in Fig. 3.8. The measured results agree with the simulated results except for small frequency offset. The a little frequency deviation may be caused by the underestimation of the substrate dielectric constant. In this structure, good input impedance is achieved by using quarter wave transformers. Moreover, good isolation is achieved by using the inset feeds. The measured 10-dB impedance bandwidth of port 1 and port 2 are 1.81% (5.742~5.847 GHz) and 1.74% (5.743~5.844 GHz) respectively. The isolation between two input ports is better than 15 dB in this bandwidth.

The normalized simulated and measured radiation patterns at dip point are shown in Fig. 3.9 and Fig. 3.10, respectively. The measured radiation patterns are similar to the simulated results. The radiation patterns are not perfect symmetry along the z-axis due to the perturbation from the microstrip lines. From this result, satisfying cross-polarization level and high gain is obtained. Because the edge of oversize antenna is larger than conventional patch antenna, the broadside peak realized gain is higher

than the conventional design. Unfortunately, the oversize edge is greater than $\lambda_0/2$ that causes despairing side lobe level. The detailed analysis is reported in [14]. Fig. 3.11 and Fig. 3.12 show the measured and simulated peak realized gain of patch antenna excited from port 1 and port 2 respectively. The measured peak realized gain are in the range of 6.6~8.3 dBic for RHCP excited by port 1 and 7.1~9.3 dBic for LHCP excited by port2, respectively. Furthermore, the measured and simulated radiation efficiency is also shown in Fig. 3.13 and Fig. 3.14. The measured radiation efficiencies are in the range of 58%~69% for both port1 and port 2. Both simulated and measured axial ratio bandwidth for RHCP and LHCP at broadside direction is shown in Fig. 3.15 and Fig. 3.16. The measured axial ratio bandwidth of port 1 and port 2 are 0.96% (5.745~5.8 GHz) and 0.95% (5.75~5.805 GHz) respectively. The axial ratio beam width for RHCP and LHCP are shown in Fig. 3.17 and Fig. 3.18. The measured axial ratio beam width of port 1 is from -14° to 32° at X-Z plane and from -21° to 23° at Y-Z plane. However, the measured axial ratio beam width of port 2 is from 0° to 23° at X-Z plane and from -18° to 32° at Y-Z plane. The difference of axial ratio beam width between port 1 and port 2 may be due to a little observational error.

3.3 An Dual-Feed Dual Circularly Polarized Oversize Patch Antenna with Taper Line

3.3.1 Antenna Design and Analysis

In the previous section, an oversize dual circular polarized patch antenna matched by quarter wave transformers is presented. The 10-dB impedance bandwidth for port 1 and port 2 are 1.81% and 1.74% respectively. To verify the 10-dB impedance bandwidth

restricted by antenna behavior instead of impedance transformers, the impedance matching is used by tapered lines. In order to verify the bandwidth of taper line is large enough to cover the antenna bandwidth, two taper lines connect each other. The geometry and scattering parameters are shown in Fig. 3.19 and Fig 3.20. In Fig. 3.20, the reflection coefficient is about 0 dB and transmission coefficient lower than -20 dB.

The geometry of the proposed antenna matched by taper line is shown in Fig. 3.21. This square patch antenna with truncated corner is also fed by two perpendicular microstrip lines directly exciting right-hand circular polarization and left-hand circular polarization at near 5.8 GHz. The simulated current distribution on the microstrip patch is shown in Fig. 3.22. For the square patch, the current forms 1.5 λ_g distribution along edges.

3.3.2   Simulation and Measurement Results

The proposed antenna is implemented and tested. The dielectric substrate is still the RO4003C with the dielectric constant $\epsilon_r = 3.55$, loss tangent $\tan\delta = 0.0027$ and thickness $h = 1.524 \, \text{mm}$. The ground plane dimension is also $70 \times 70 \, \text{mm}^2$. All simulations were gone through by software HFSS during this design procedure. All design parameters are listed in Table 3.2.

The simulated and measured S-parameters are shown in Fig. 3.23. Also, the measured results agree with the simulated results except for small frequency offset. In this structure, good input impedance is achieved by using taper lines. Similarly, good isolation is achieved by using the inset feeds. The measured 10-dB impedance bandwidth of port 1 and port 2 are 1.74% (5.75~5.851 GHz) and 1.76% (5.751~5.853 GHz) respectively. These measured results are about the same as the antenna matched by quarter wave transformers. Therefore, it can be proved that the impedance bandwidth

is restricted by antenna rather than matching transformers. Again, the isolation between two input ports is better than 15 dB in this bandwidth.

The normalized simulated and measured radiation patterns at 5.8 GHz are shown in Fig. 3.24 and Fig. 3.25, respectively. The measured radiation patterns are similar to the simulated results. The radiation patterns are not perfect symmetry along the z-axis due to the perturbation from the microstrip lines. The measured and simulated peak realized gain of patch antenna excited from port 1 and port 2 are shown in Fig. 3.26 and Fig. 3.27 respectively. The measured peak realized gain are in the range of 6.8~8.3 dBic for RHCP excited by port 1 and 7.5~9 dBic for LHCP excited by port2, respectively. In addition, the measured and simulated radiation efficiencies are shown in Fig. 3.28 and Fig. 3.29. The measured radiation efficiencies are in the range of 56%~70% for port1 and 57%~68% for port 2 respectively. Both simulated and measured axial ratio bandwidth for RHCP and LHCP at broadside direction is shown in Fig. 3.30 and Fig. 3.31. The measured in-band axial ratio bandwidth of port 1 and port 2 are 0.87% (5.75~5.8 GHz) and 1.21% (5.75~5.82 GHz) respectively. The axial ratio beam width for RHCP and LHCP are shown in Fig. 3.32 and Fig. 3.33. The measured axial ratio beam width of port 1 is from -5° to 7° at X-Z plane and from -27° to 24° at Y-Z plane. Also, the measured axial ratio beam width of port 2 is from -9° to 28° at X-Z plane and from -18° to 22° at Y-Z plane.

3.4 Conclusion

In this chapter, oversize dual-feed dual circularly polarized patch antennas have been presented. Comparing with the conventional design, the realized gain is improved by operated at TM_{30} mode. This design has higher gain than conventional antenna

without using array forms, but it may cause unwanted side lobe. The 10-dB impedance bandwidth is restricted by antenna itself through changing matching transformers. Up to 15 dB isolation can be achieved by using inset feeds.
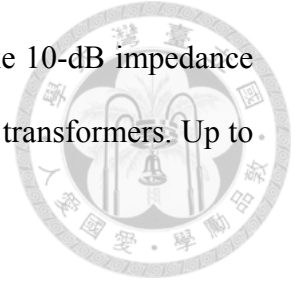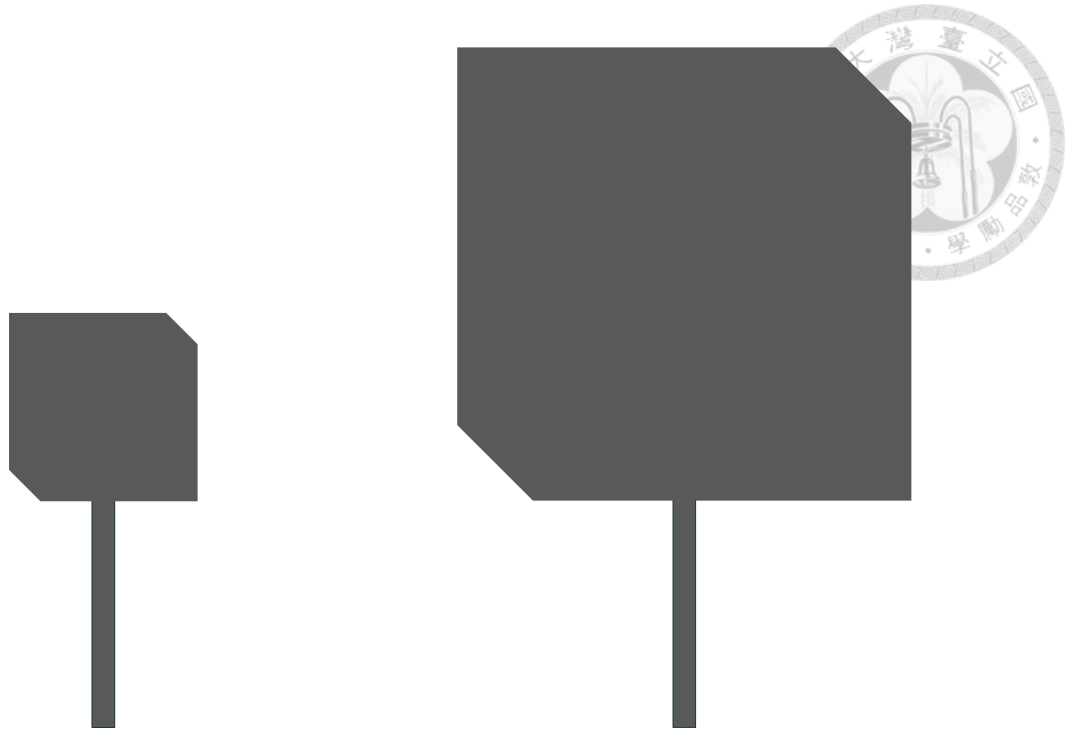
Fig. 3.1 Circularly polarized patch antenna operating at TM_{10} mode and TM_{30} mode
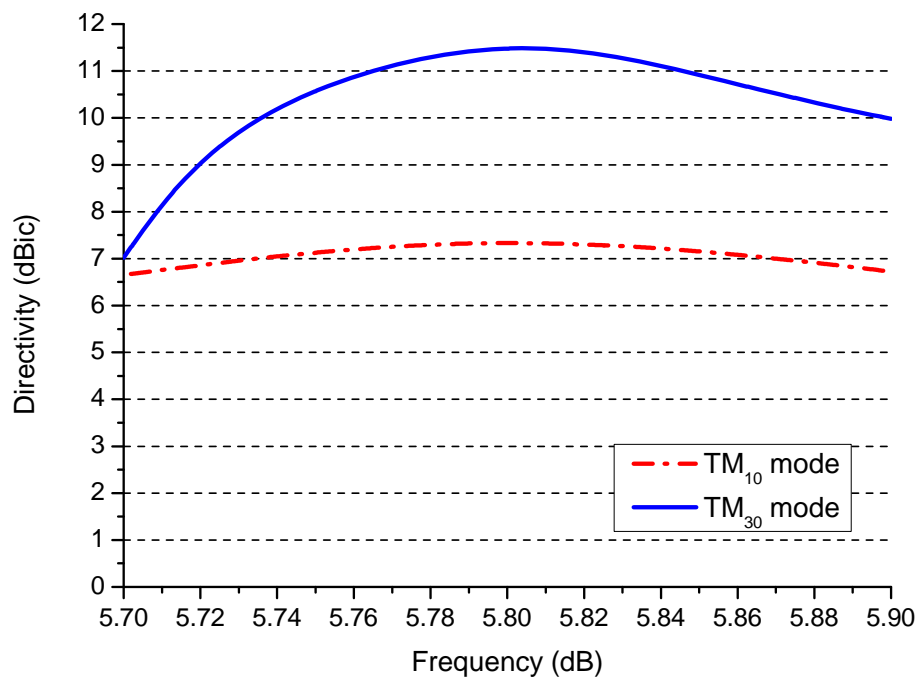
Fig. 3.2 Simulated directivity of TM_{10} mode and TM_{30} mode

Fig. 3.3 Electric field lines for microstrip line
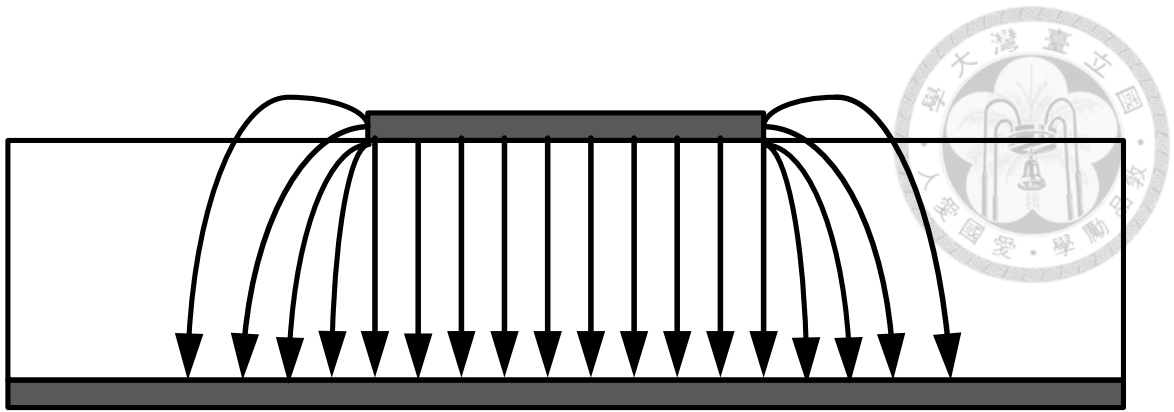
Coupling
$E_1 \cdot E_2$
$H_1 \cdot H_2$

Resonator 01	Resonator 02
E_1	E_2
H_1	H_2
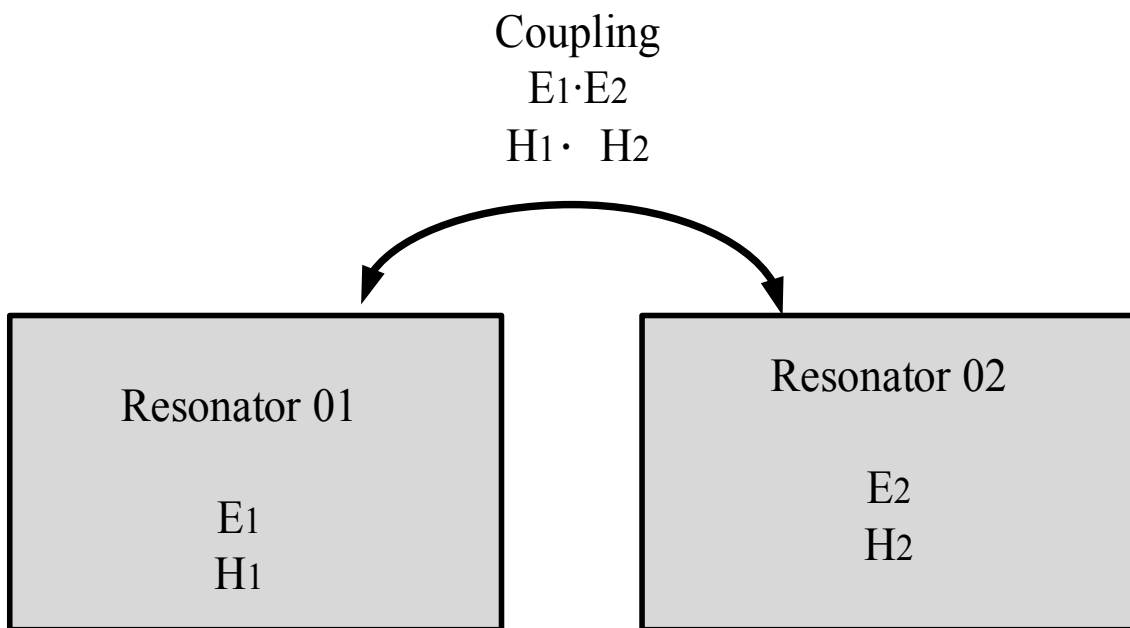
Fig. 3.4 General coupled RF/microwave resonators
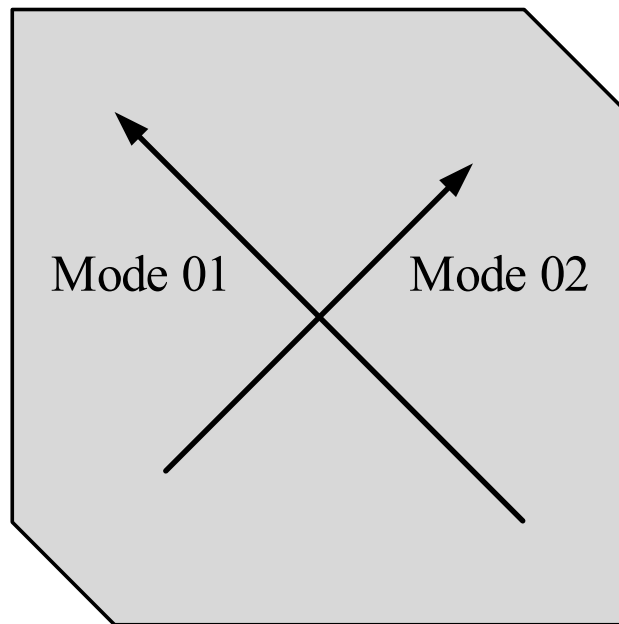
Fig. 3.5 Orthogonal modes in circular polarized microstrip patch operated at

fundamental mode
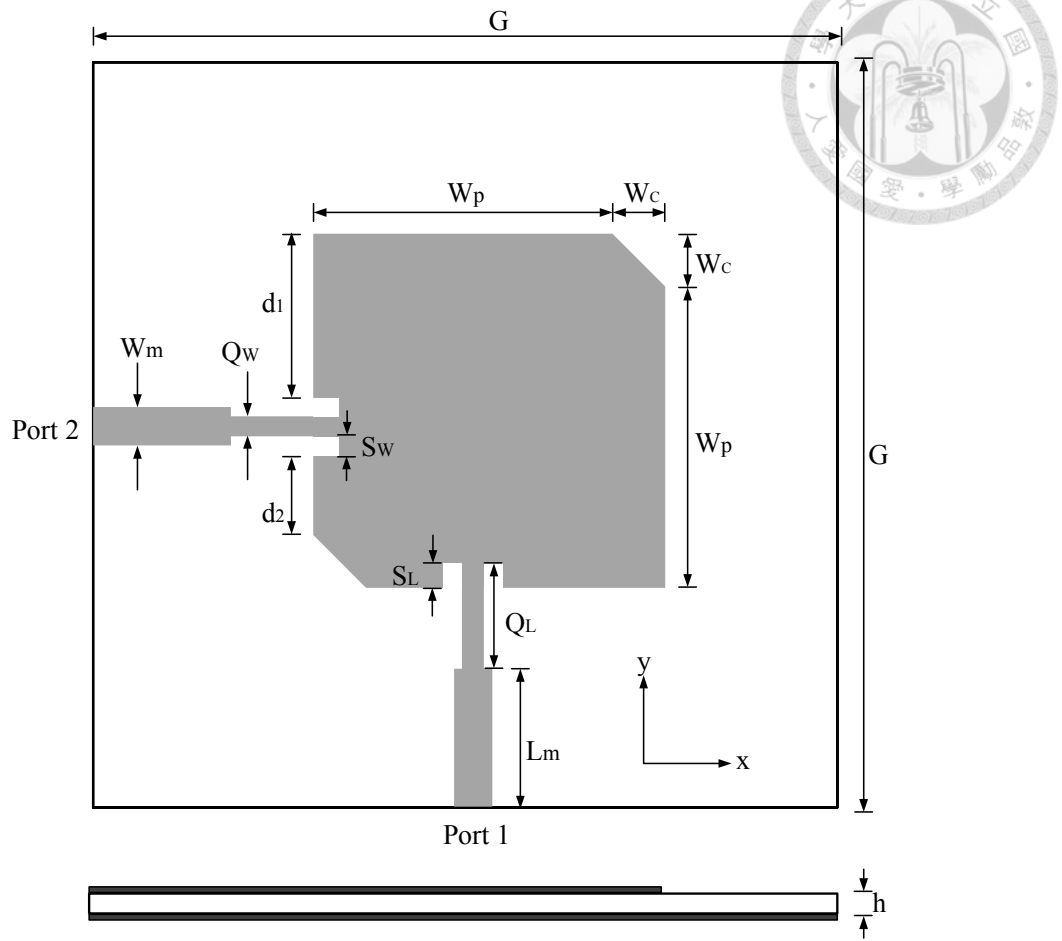
Fig. 3.6 Geometry of the dual circularly polarized TM_{30} mode patch antenna with

quarter wave transformers

Design Parameters (Unit : mm)			
G	h	W_p	W_c
70	1.524	35.1	4.8
d_1	d_2	S_L	S_W
18.2	9.8	2.7	2.8
Q_L	Q_W	L_m	W_m
7.7	1.5	10.05	3.45

Table 3.1 Design parameters of the TM_{30} mode patch antenna with quarter wave

transformers

(a) Phase = 0°

(b) Phase = 90°

35
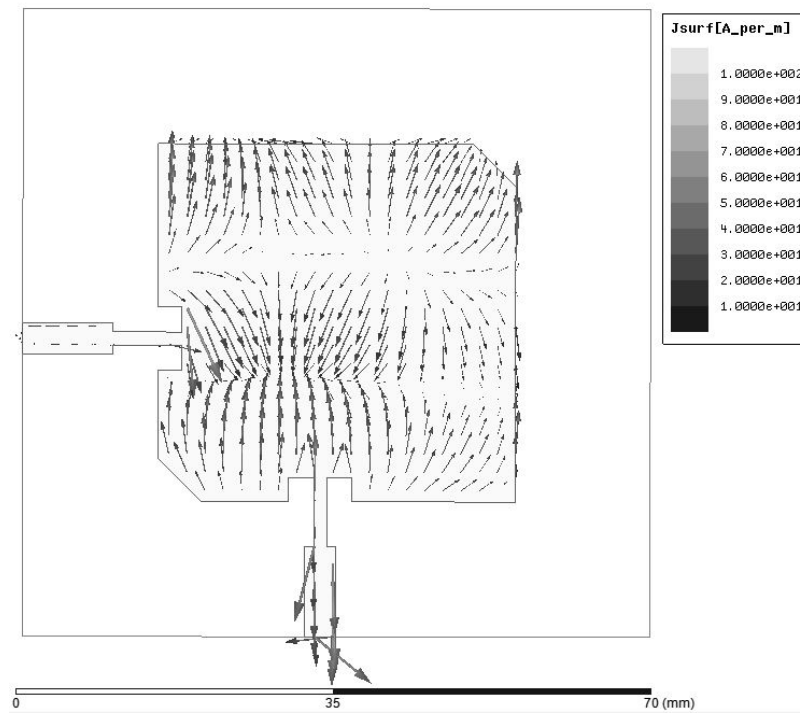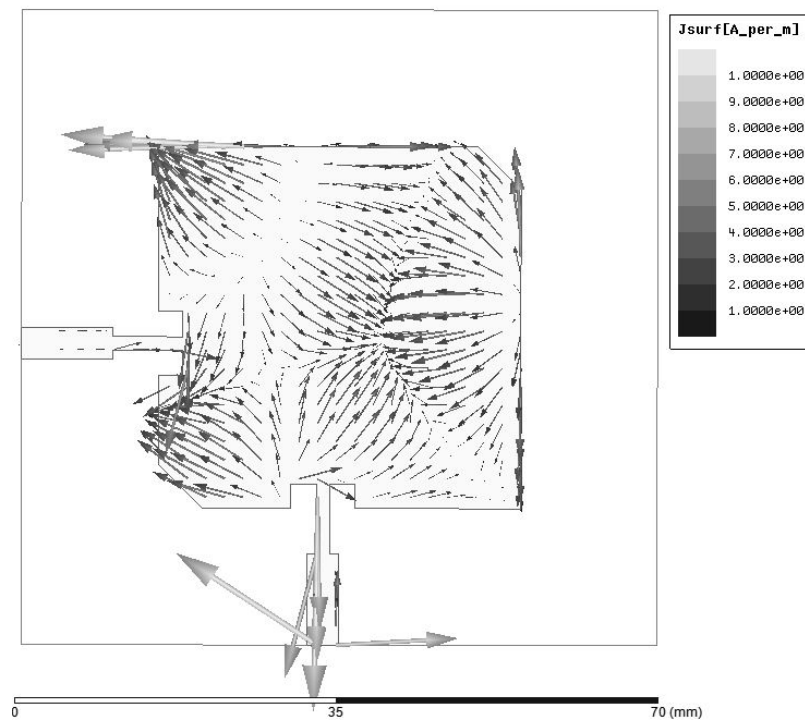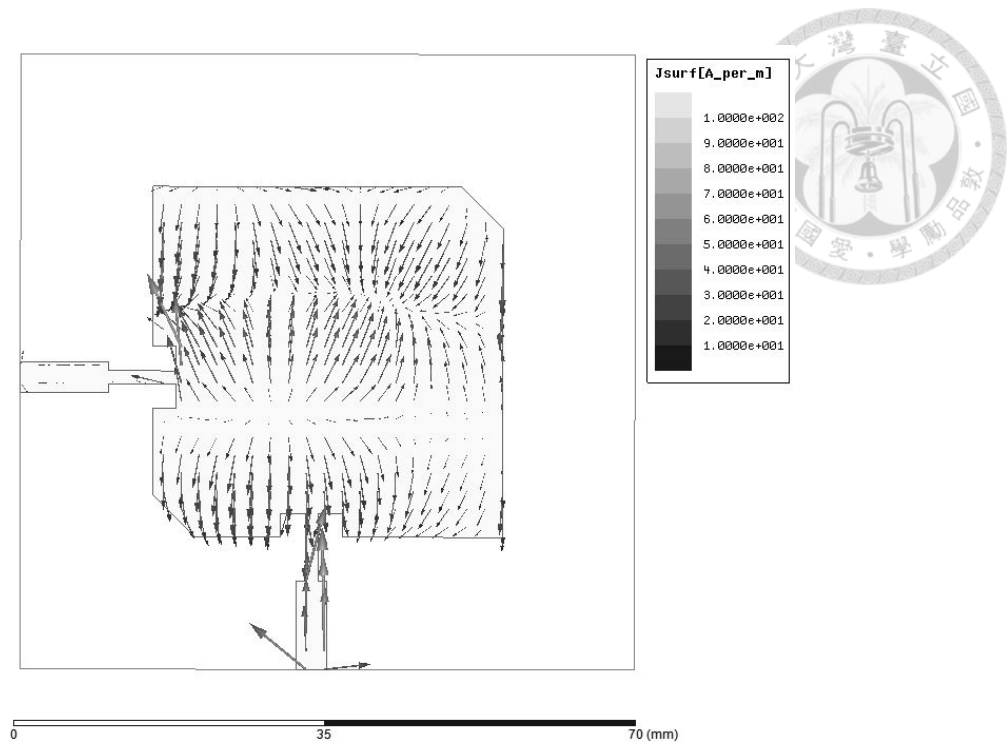
(c) Phase = 180°
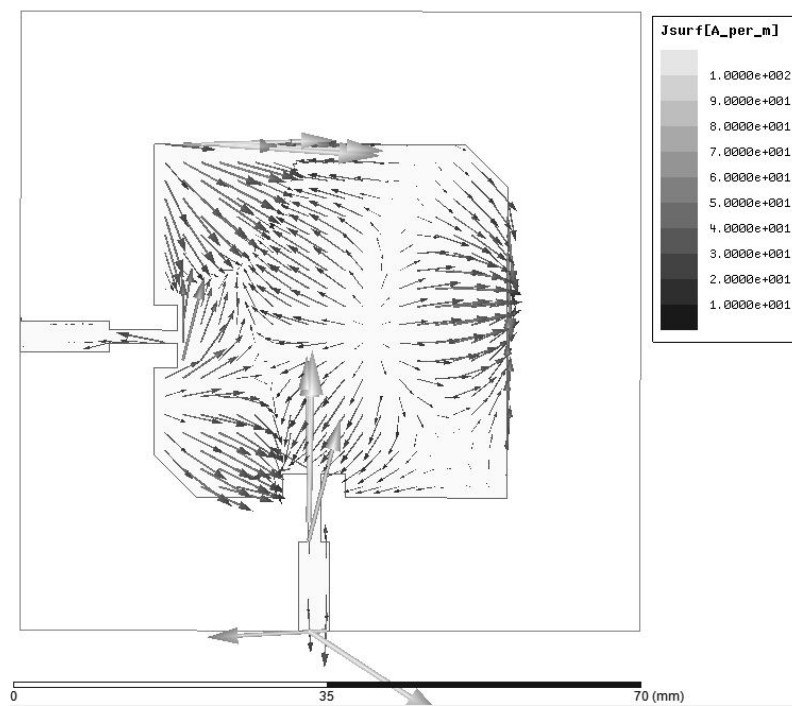
(d) Phase = 270°

Fig. 3.7 Current distribution
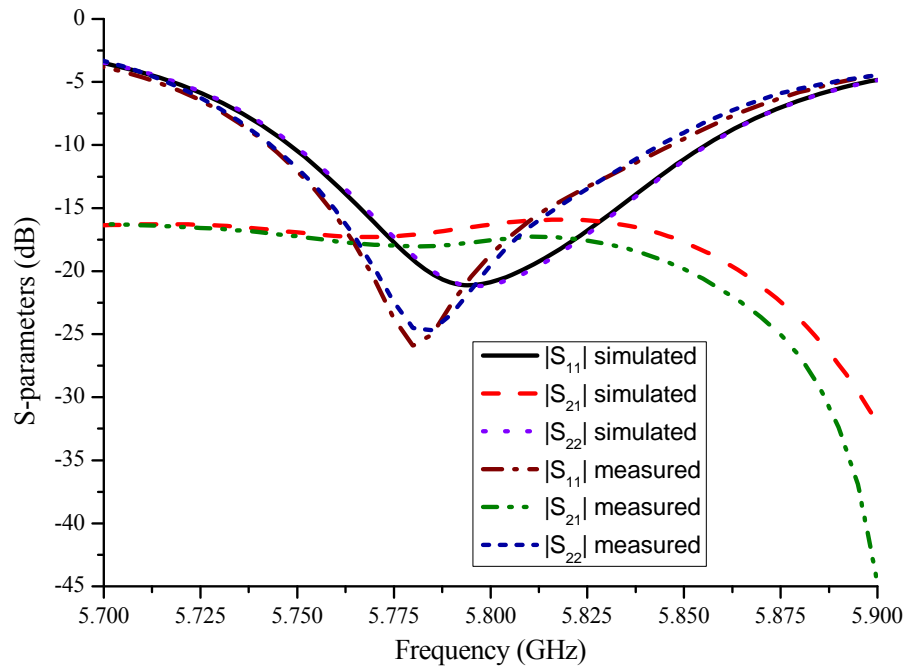
Fig. 3.8 Simulated and measured S-parameters of the TM_{30} mode patch antenna with

quarter wave transformers
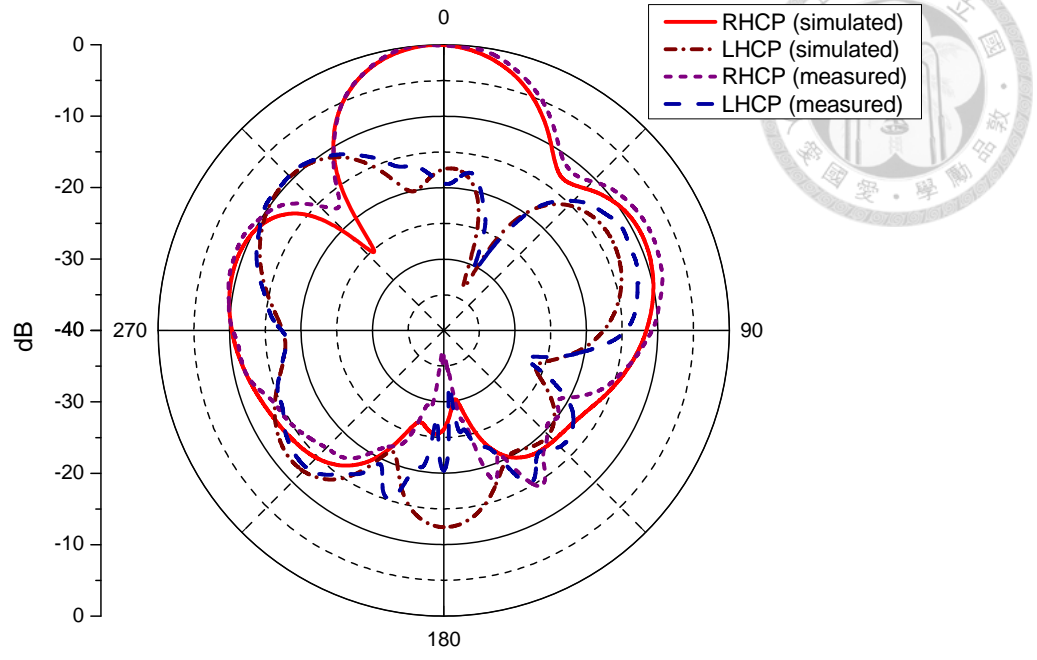
(a) X-Z plane
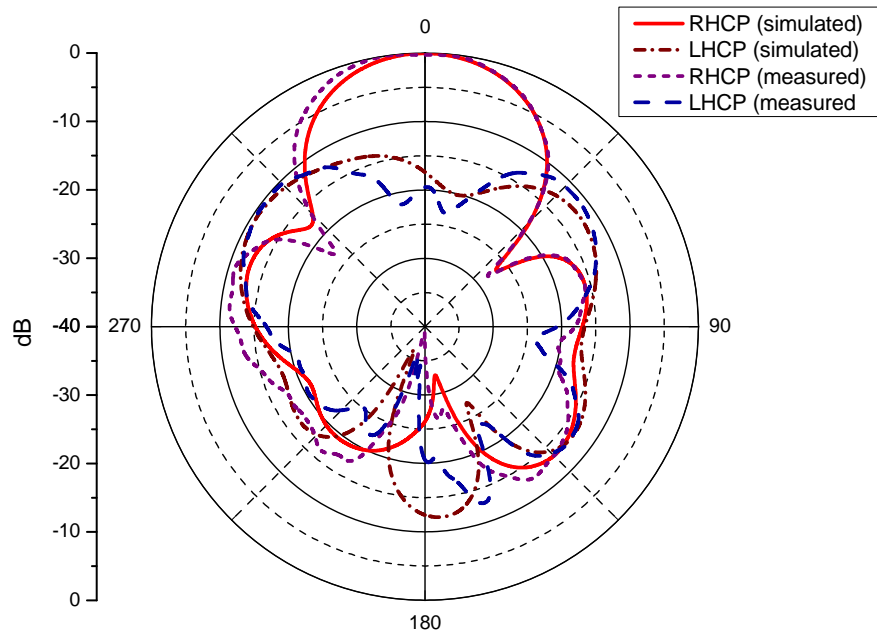
(b) Y-Z plane

Fig. 3.9 Simulated and measured normailzed radiation patterns of the proposed

antenna matched by quarter wave transformers (Port 1 excited)

38
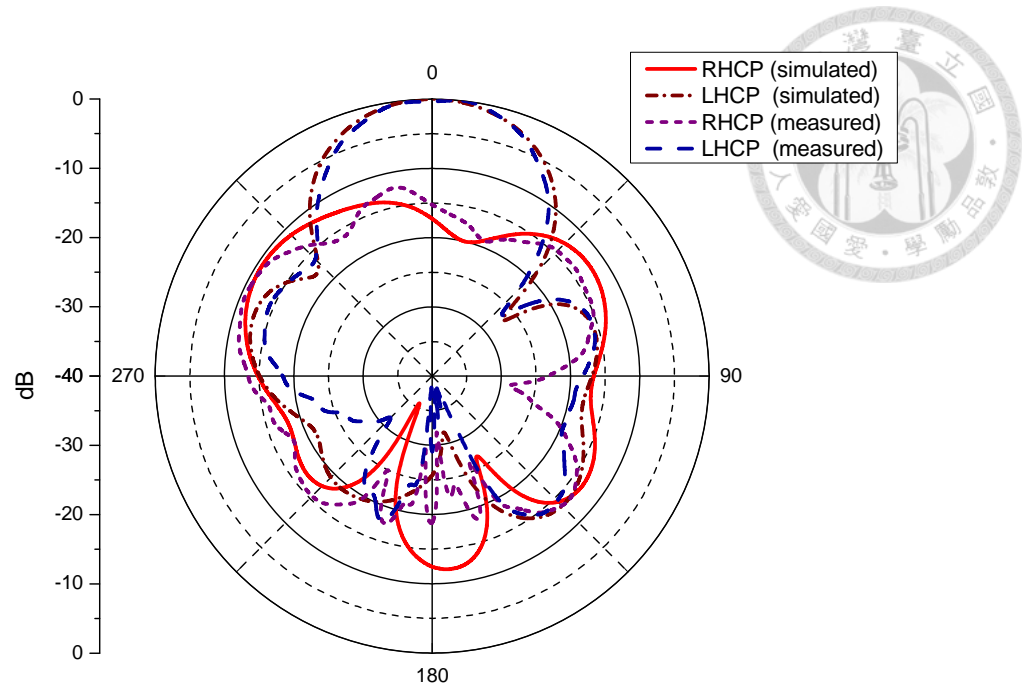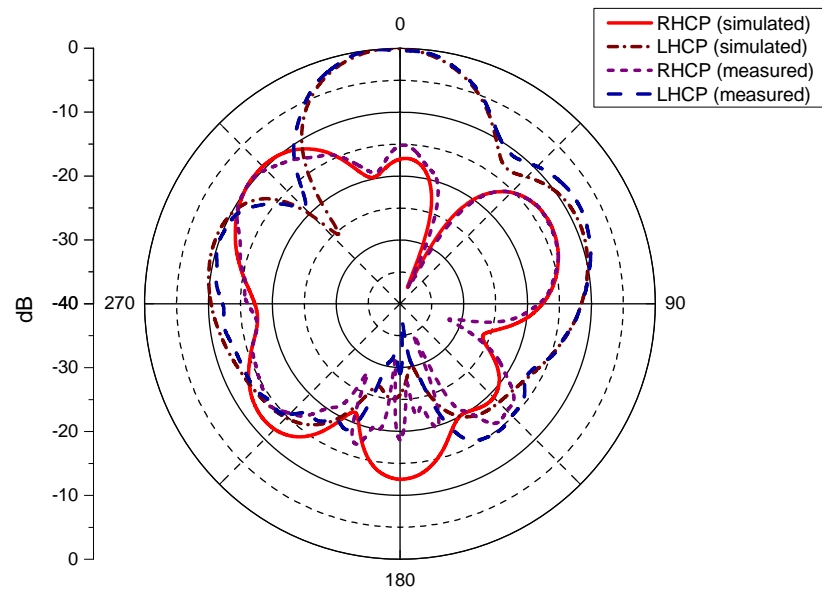
(a) X-Z plane

(b) Y-Z plane

Fig. 3.10 Simulated and measured normailzed radiation patterns of the proposed

antenna matched by quarter wave transformers (Port 2 excited)
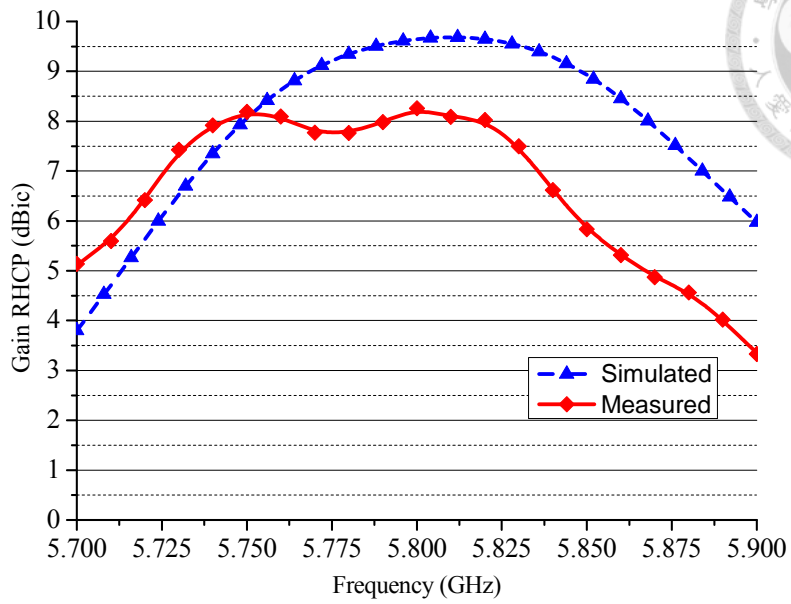
Fig. 3.11 Simulated and measured peak realized gain of RHCP with quarter wave
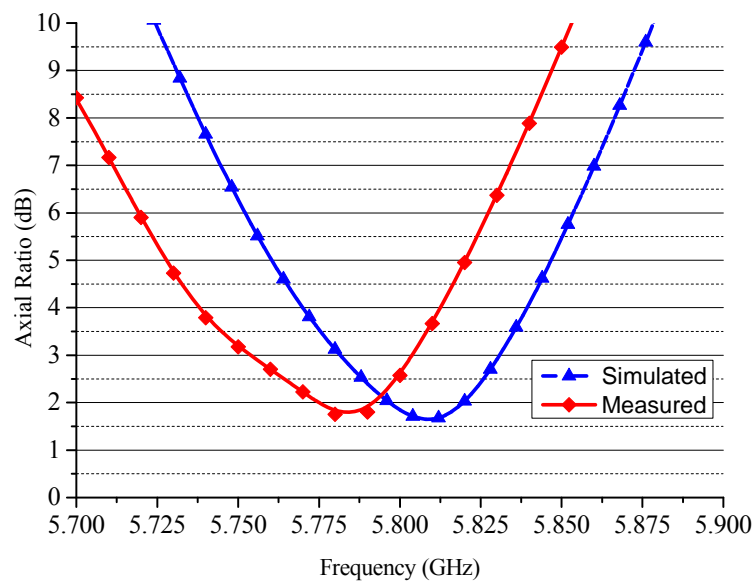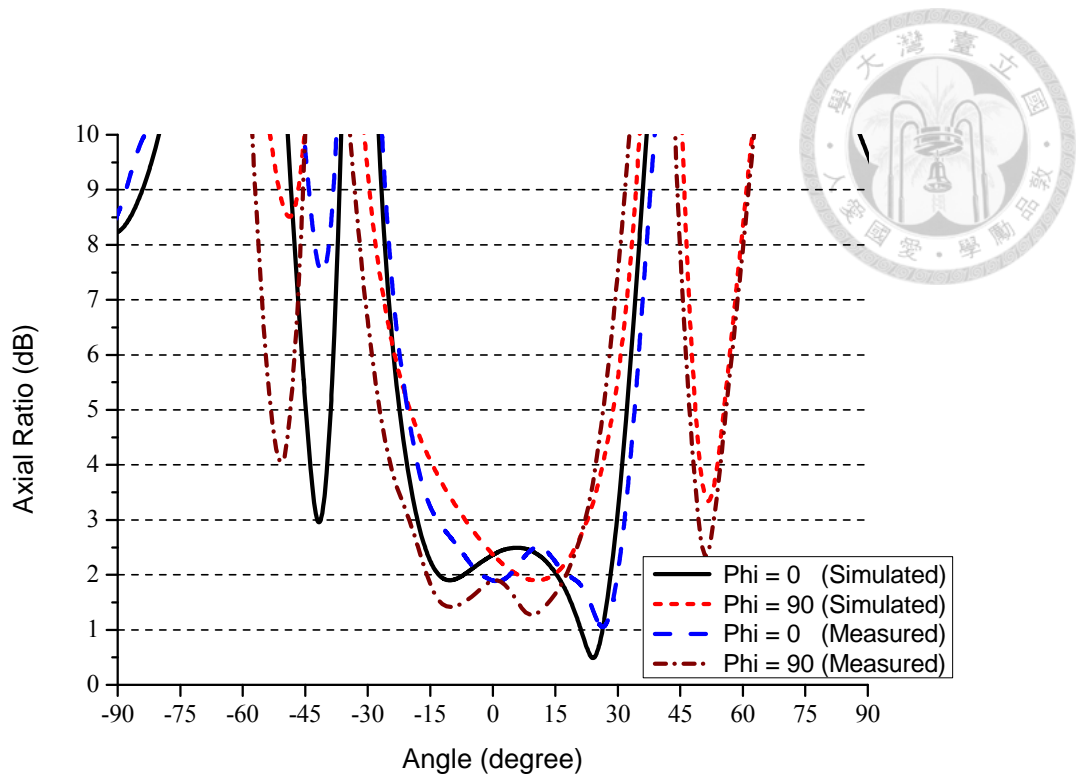
transformers (Port 1 excited)
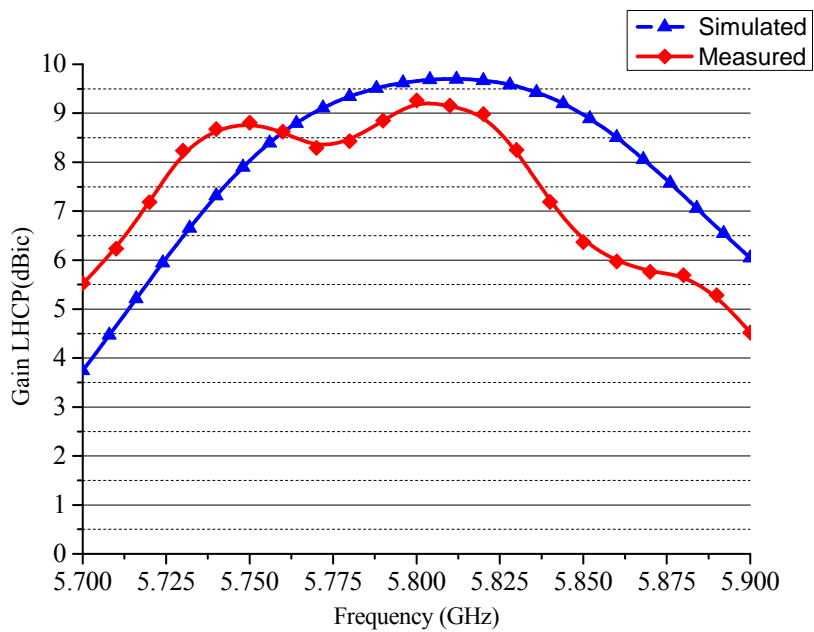
Fig. 3.12 Simulated and measured peak realized gain of LHCP fed by quarter wave

transformers (Port 2 excited)
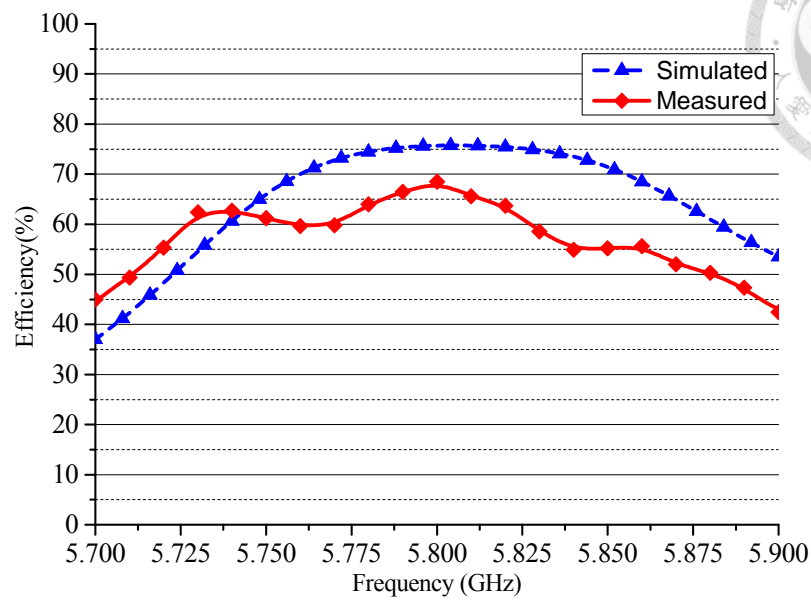
Fig. 3.13 Simulated and measured radiation efficiency of RHCP with quarter wave

transformers (Port 1 excited)
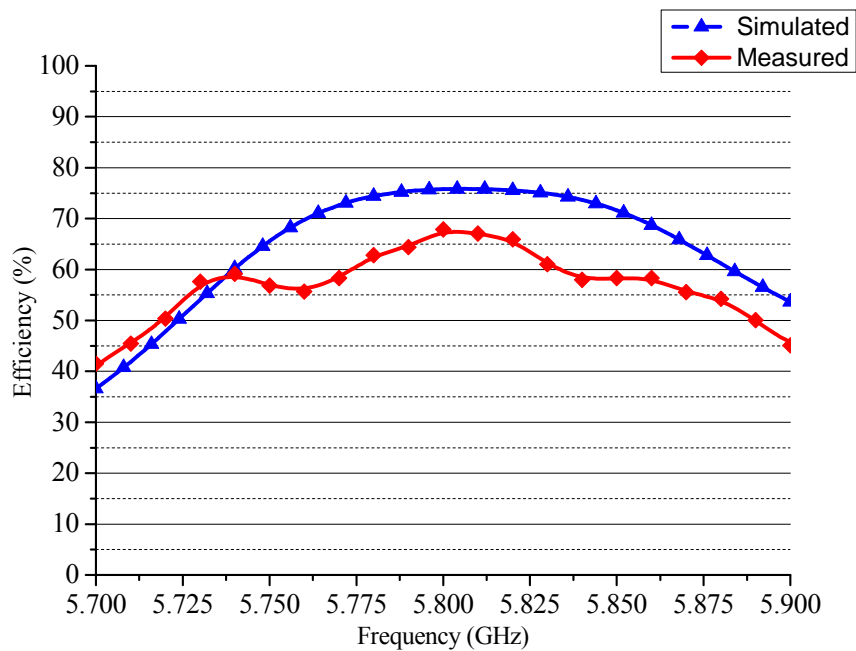
Fig. 3.14 Simulated and measured radiation efficiency of LHCP with quarter wave

transformers (Port 2 excited)
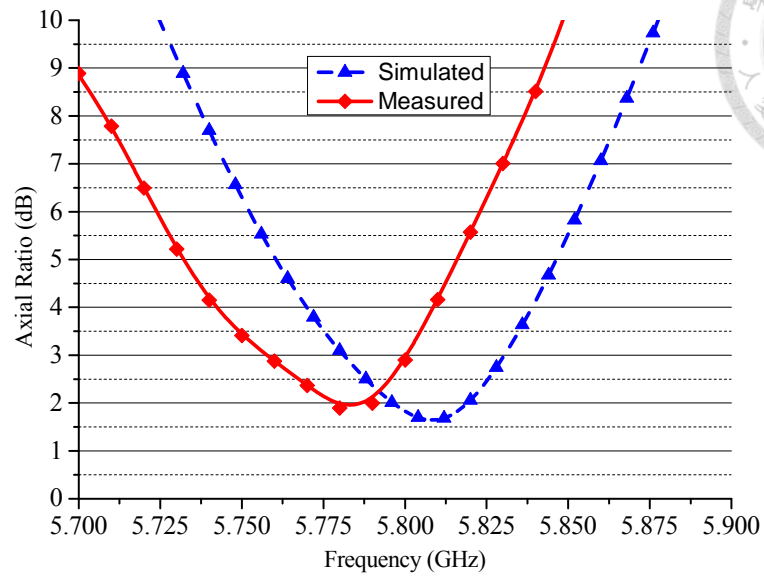
Fig. 3.15 Simulated and measured axial ratio of RHCP with quarter wave transformers
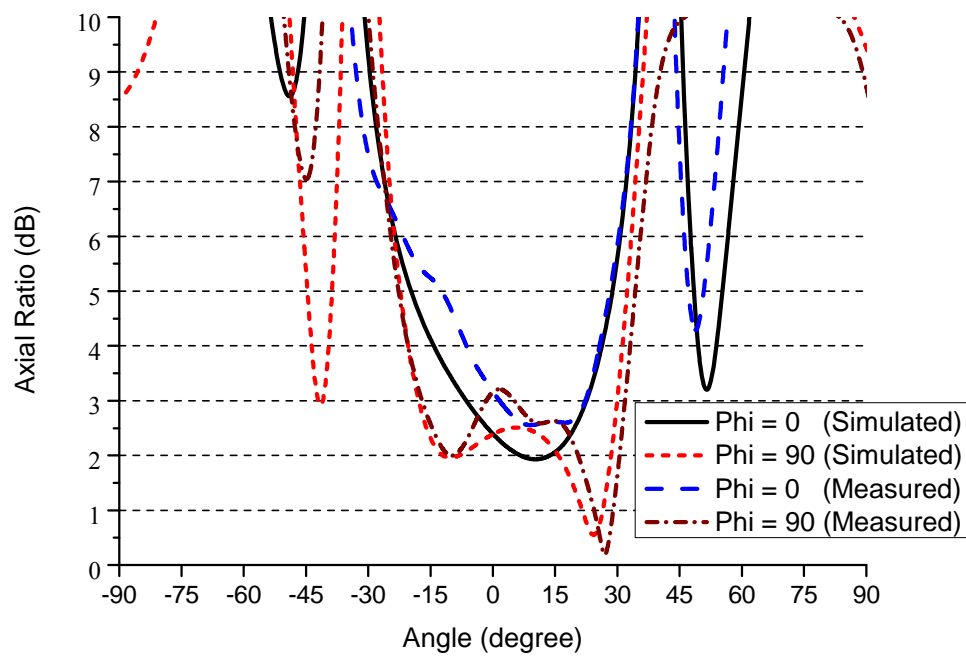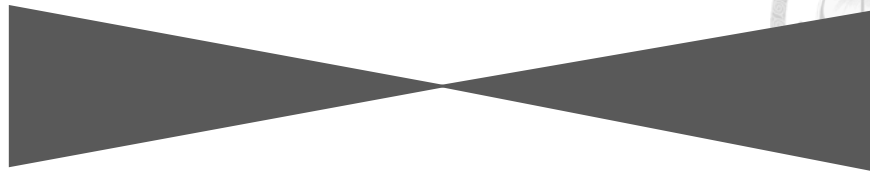
(Port 1 excited)

Fig. 3.16 Simulated and measured axial ratio of LHCP with quarter wave transformers

(Port 2 excited)

Fig. 3.17 Simulated and measured axial ratio beam width with quarter wave transformers (Port 1 excited)

Fig. 3.18 Simulated and measured axial ratio beam width with quarter wave transformers (Port 2 excited)

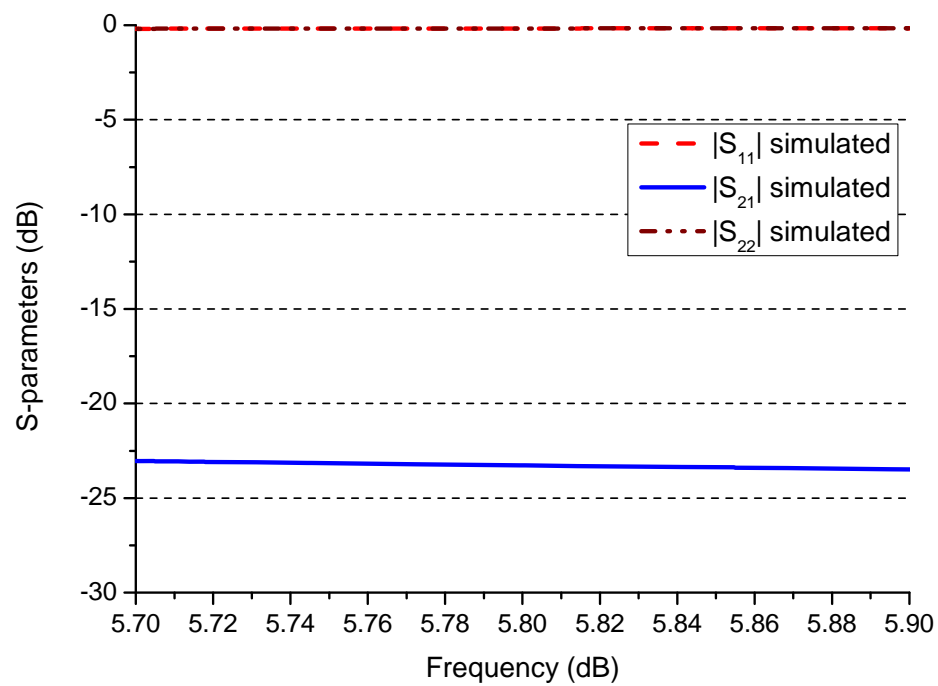Fig. 3.19 Geometry of two taper line connected together

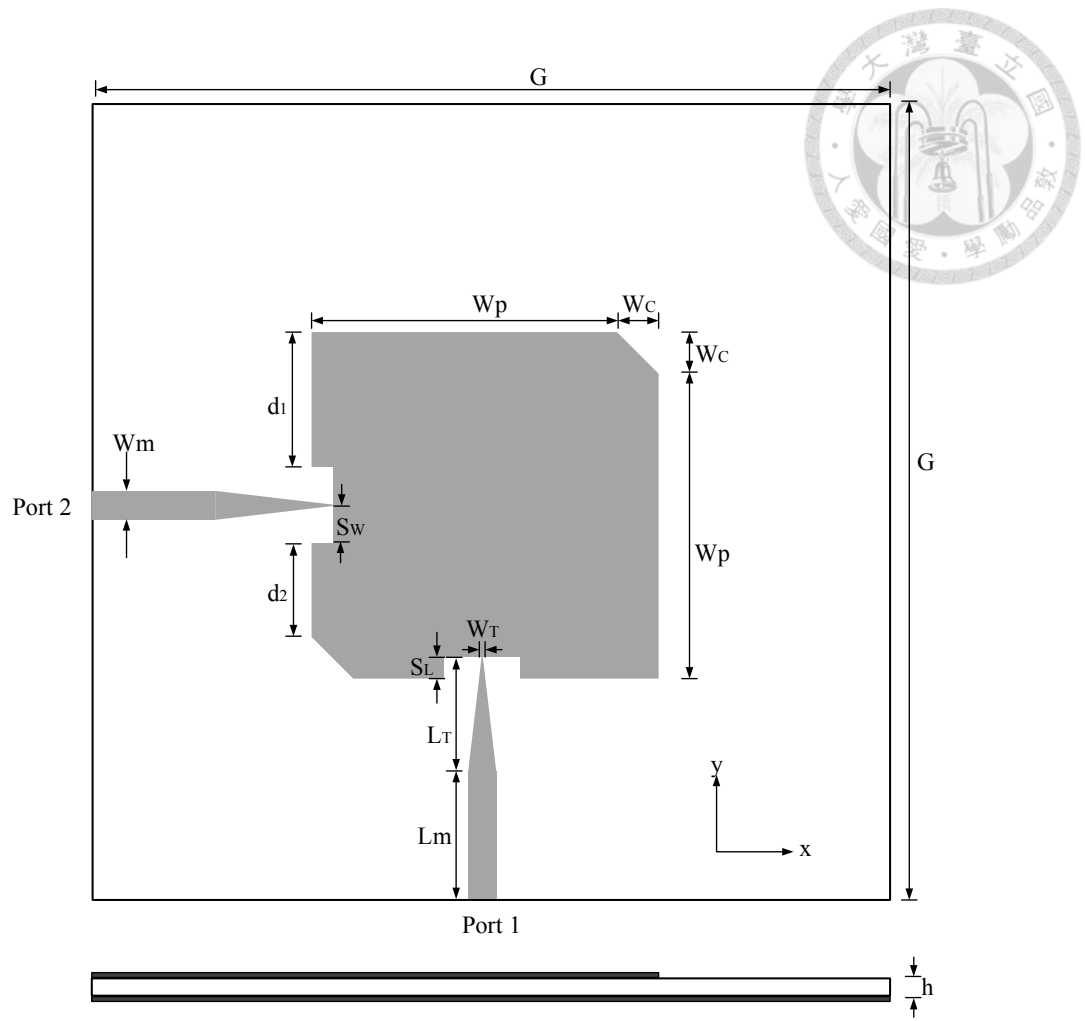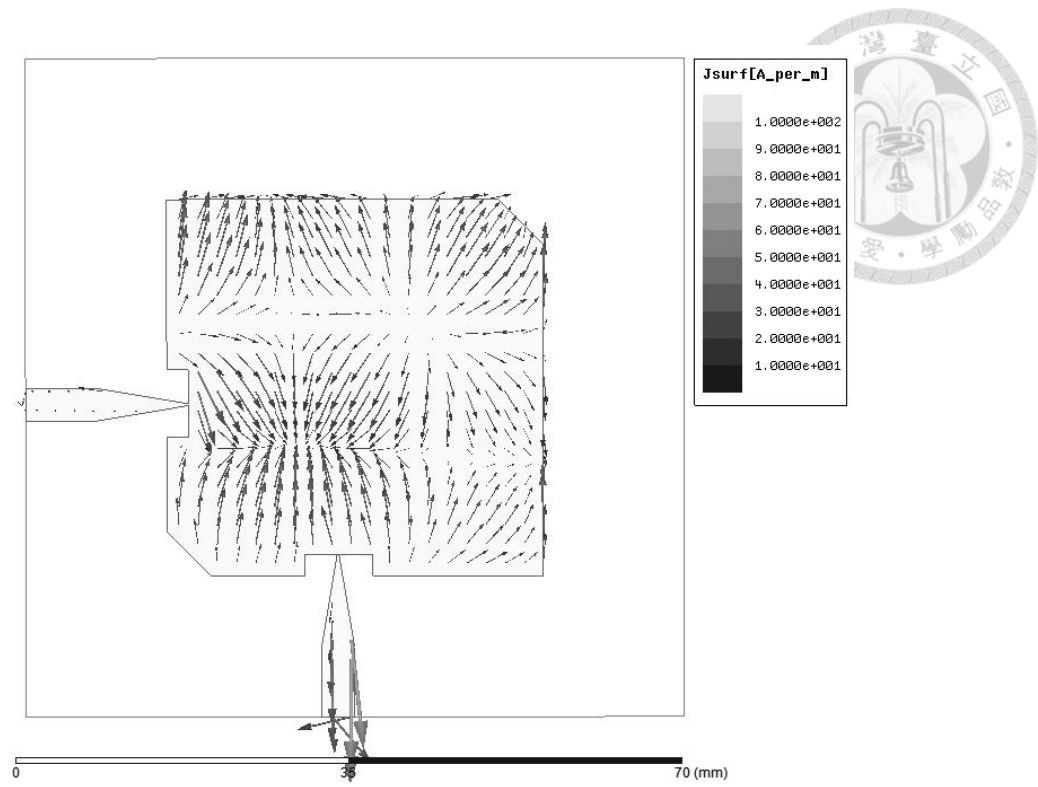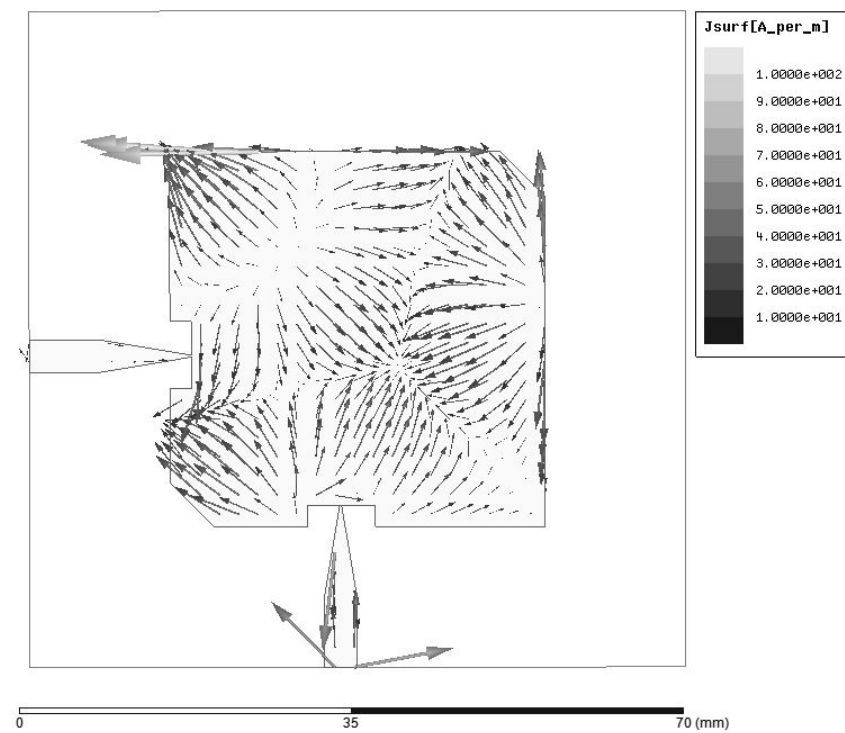Fig. 3.20 S-parameters of two taper lines connected together

Fig. 3.21 Geometry of the dual circularly polarized TM_{30} mode patch antenna with

taper lines

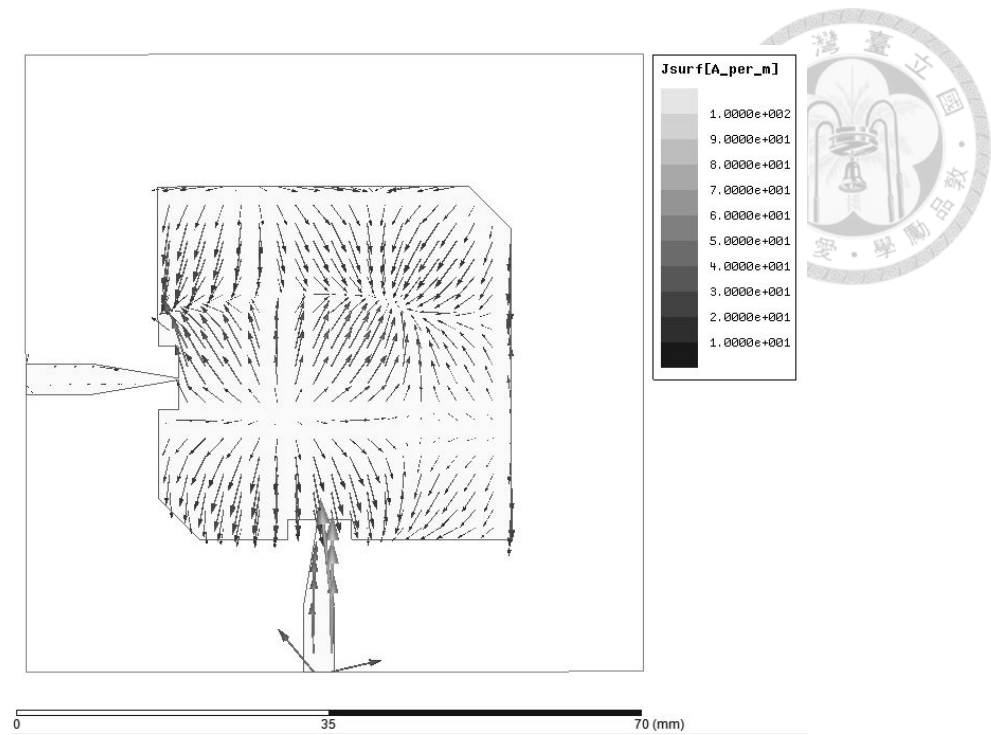| Design Parameters (Unit : mm)			
G	h	W_p	W_c
70	1.524	35.3	4.7
d_1	d_2	S_L	S_W
18.1	10	2.3	3.6
W_T	L_T	L_m	W_m
0.2	9.9	7.4	3.5

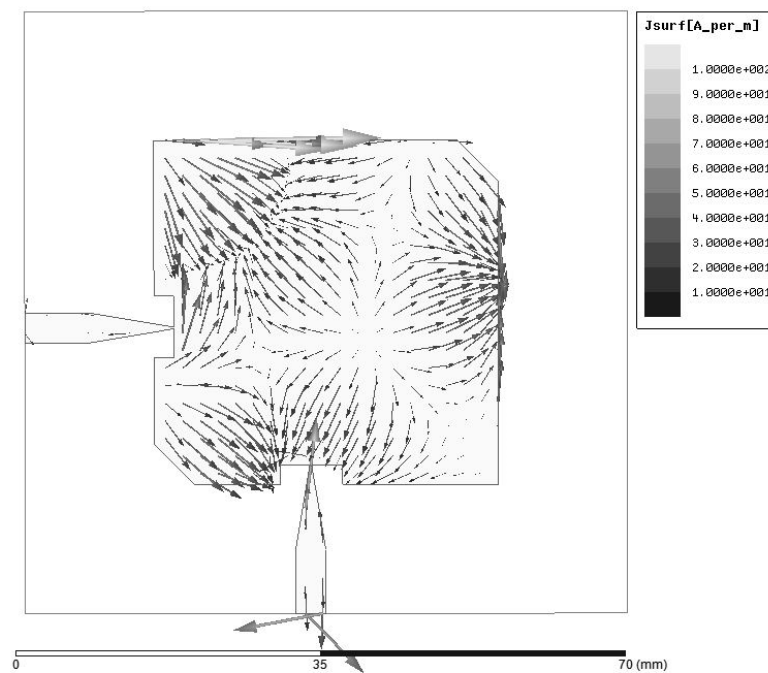Table 3.2 Design parameters of the TM_{30} mode microstrip antenna with taper lines

(a) Phase = 0°

(b) Phase = 90°

(c) Phase = 180°

(d) Phase = 270°

Fig. 3.22 Current distribution of oversize patch antenna matched by taper lines
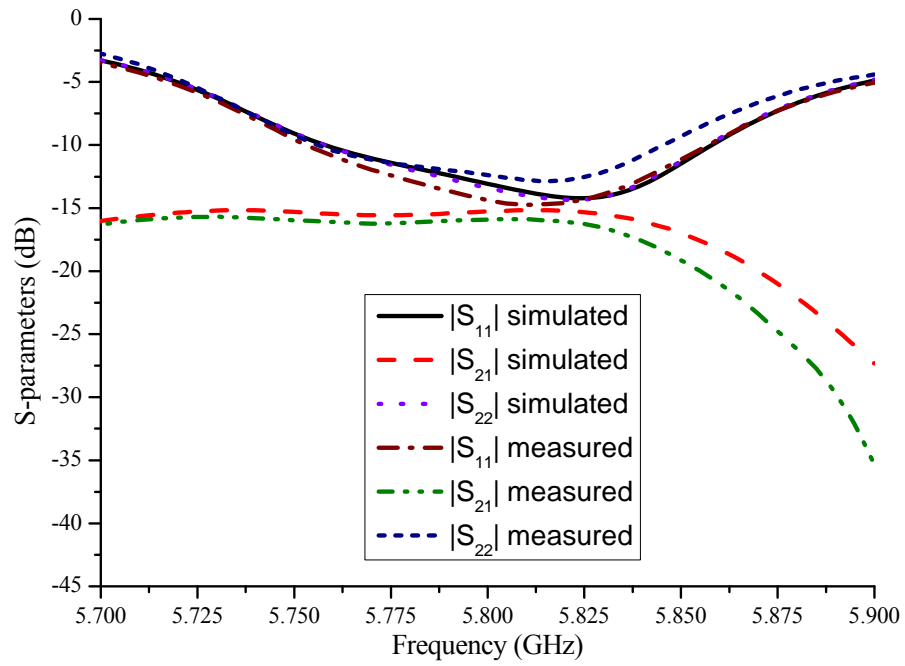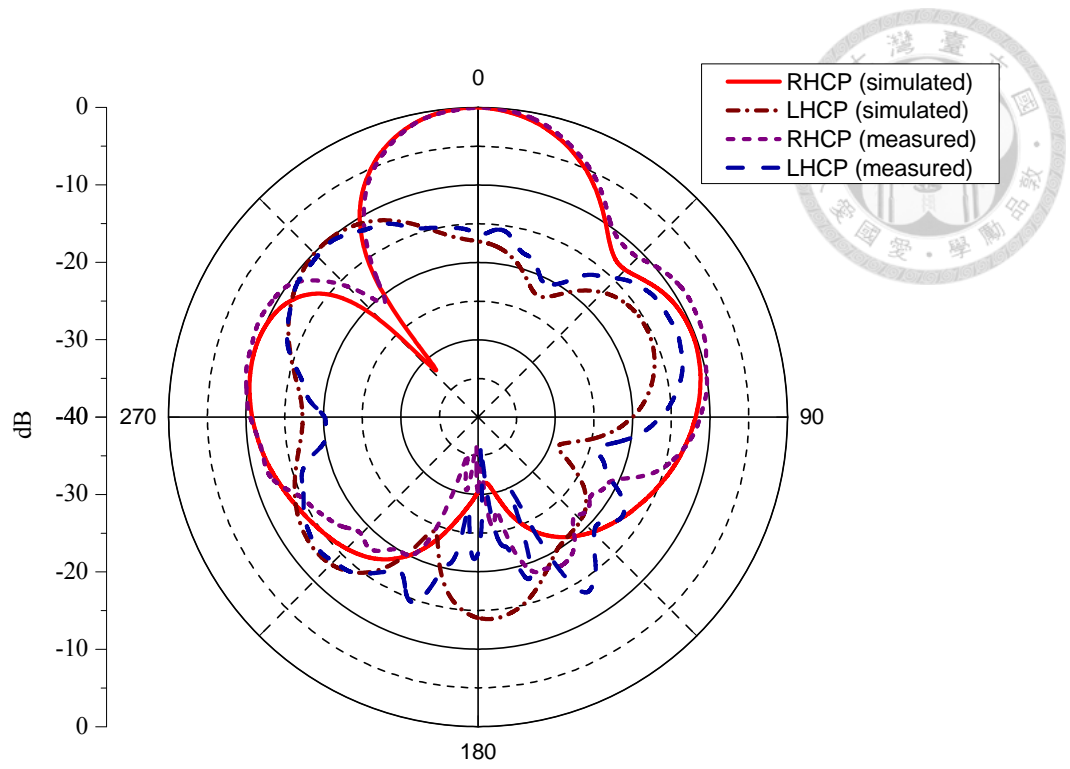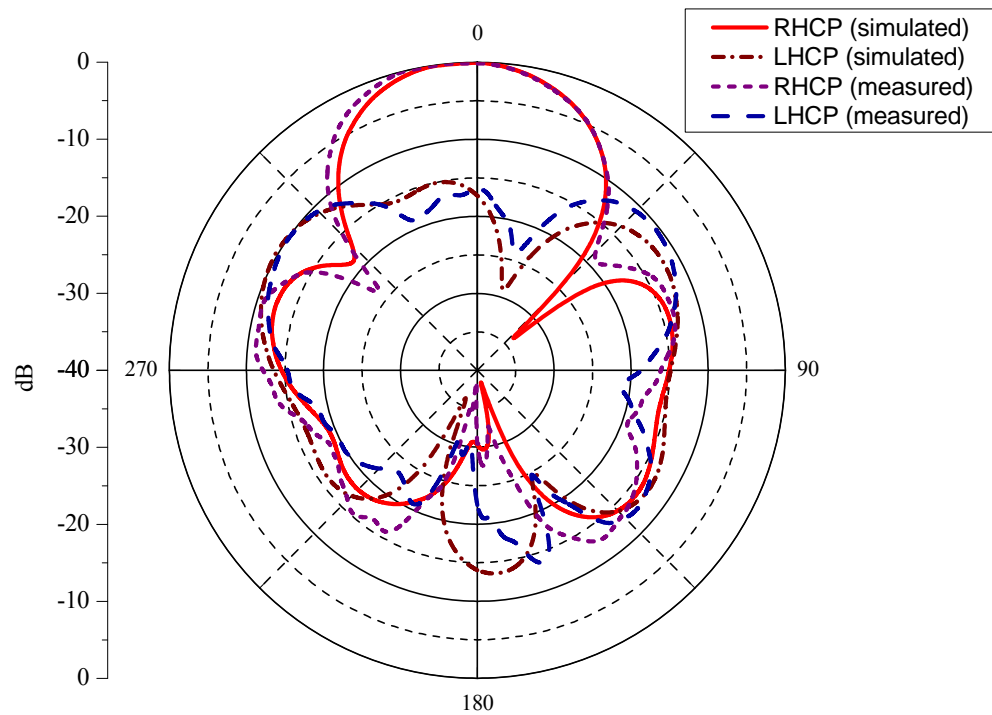
Fig. 3.23 Simulated and measured S-parameters of the TM_{30} mode microstrip antenna

with taper lines

(a) X-Z plane

(b) Y-Z plane

Fig. 3.24 Simulated and measured normailzed radiation patterns of the proposed

antenna matched by taper lines (Port 1 excited)
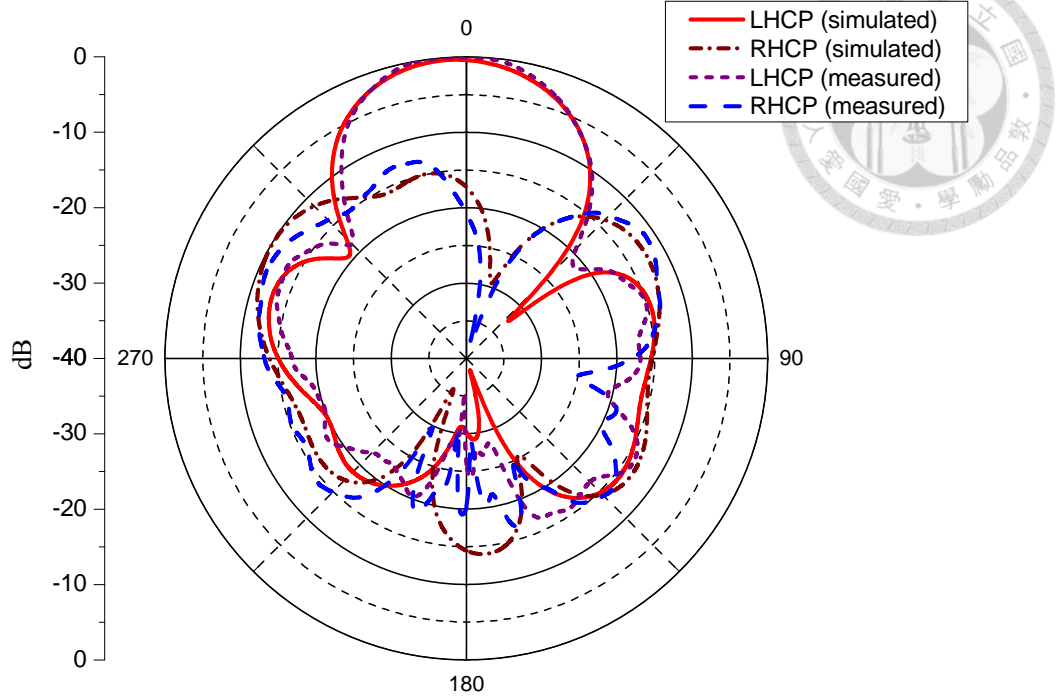
(a) X-Z plane
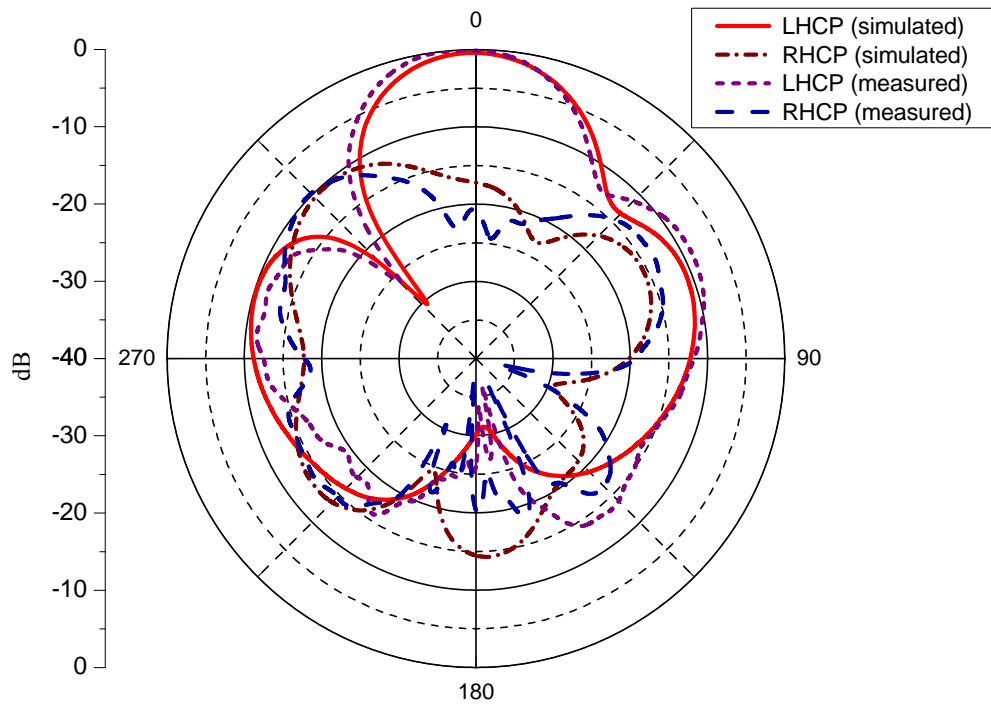

(b) Y-Z plane

Fig. 3.25 Simulated and measured normailzed radiation patterns of the proposed

antenna matched by taper lines (Port 2 excited)

50

Fig. 3.26 Simulated and measured peak realized gain of RHCP with taper lines (Port 1
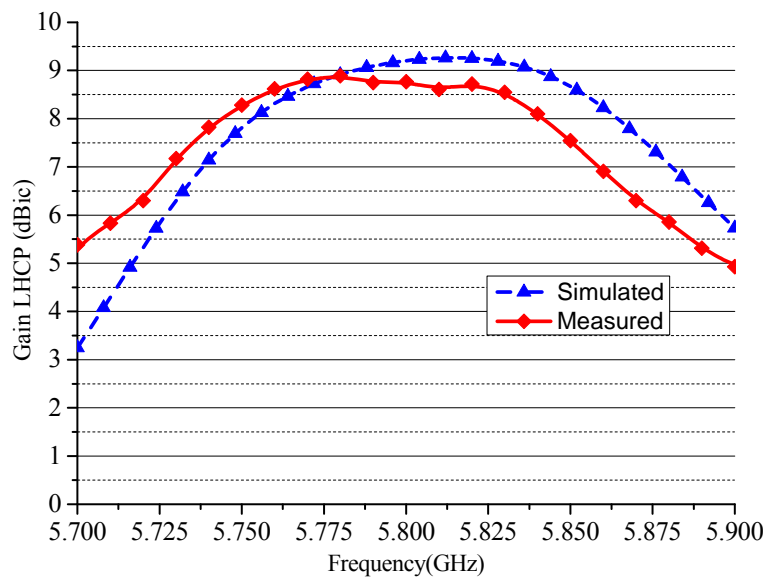
excited)

Fig. 3.27 Simulated and measured peak realized gain of LHCP with taper lines (Port 2

excited)

Fig. 3.28 Simulated and measured radiation efficiency of RHCP with taper lines (Port 1 excited)

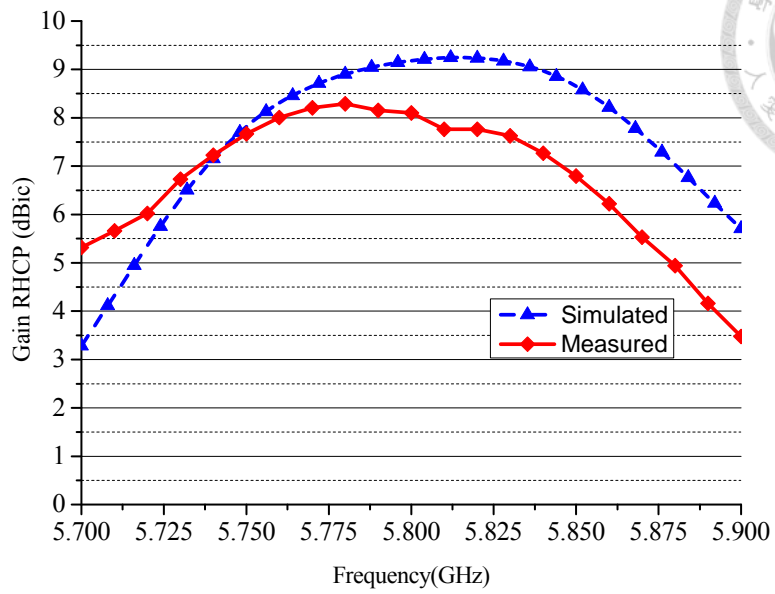Fig. 3.29 Simulated and measured radiation efficiency of LHCP with taper lines (Port 2 excited)

Fig. 3.30 Simulated and measured axial ratio of RHCP with taper lines (Port 1 excited)

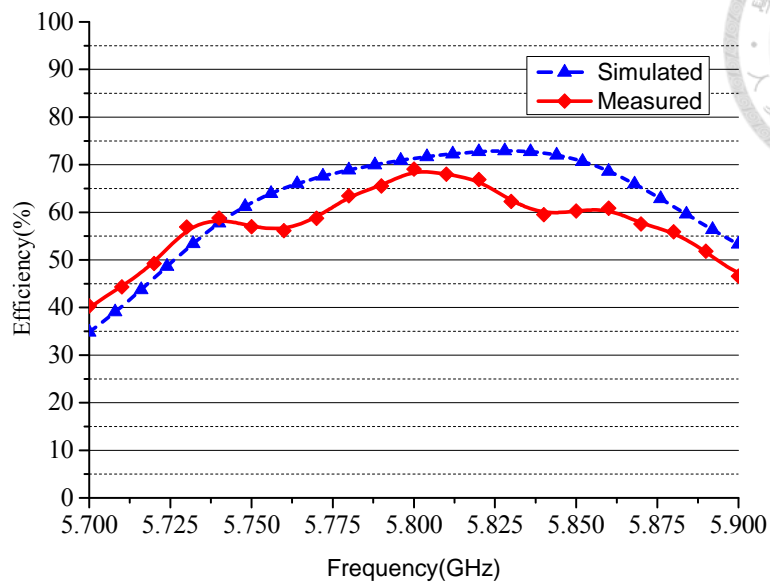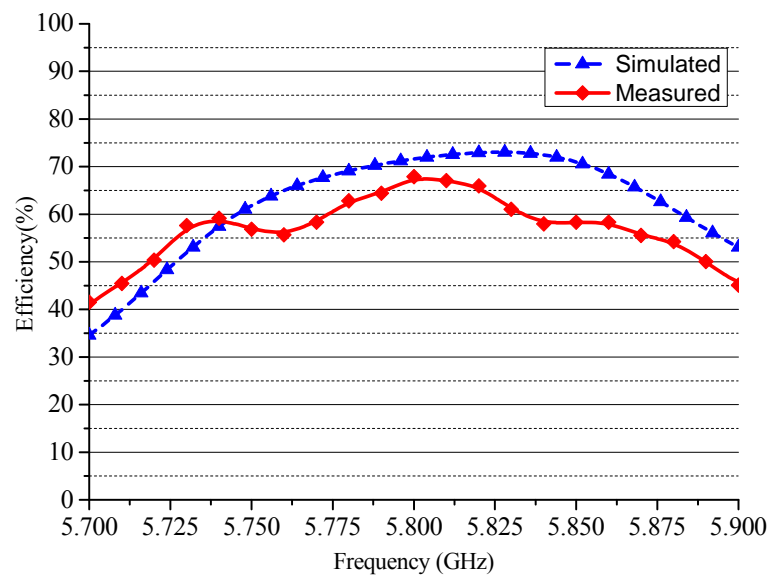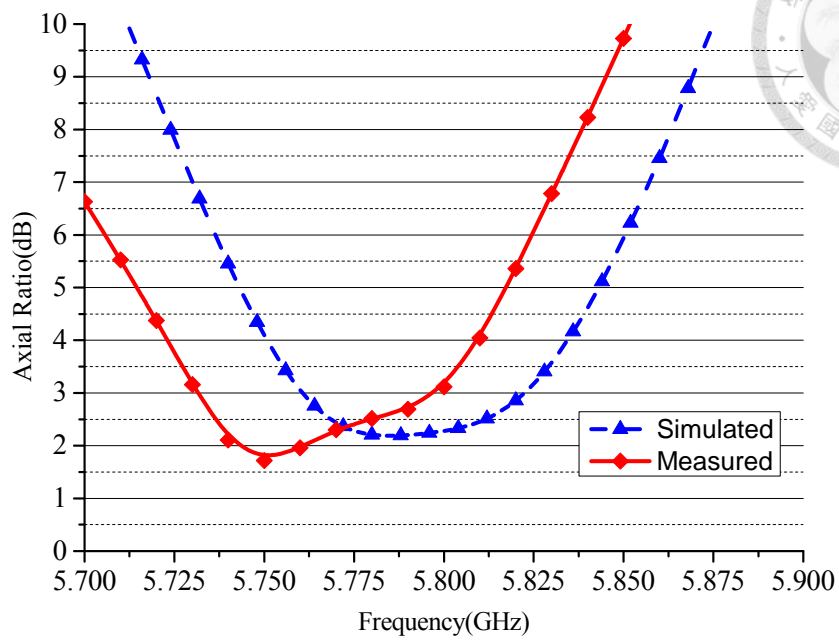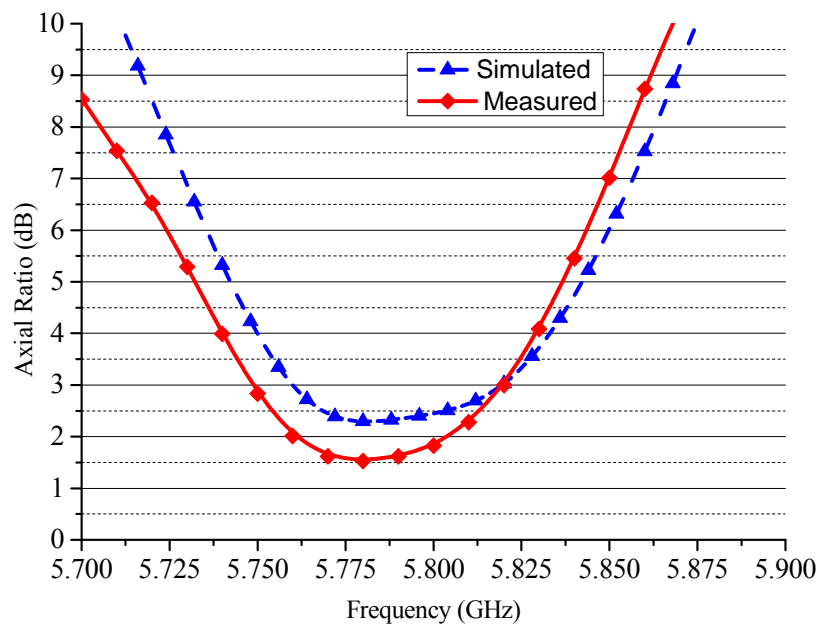Fig. 3.31 Simulated and measured axial ratio of LHCP with taper lines (Port 2 excited)
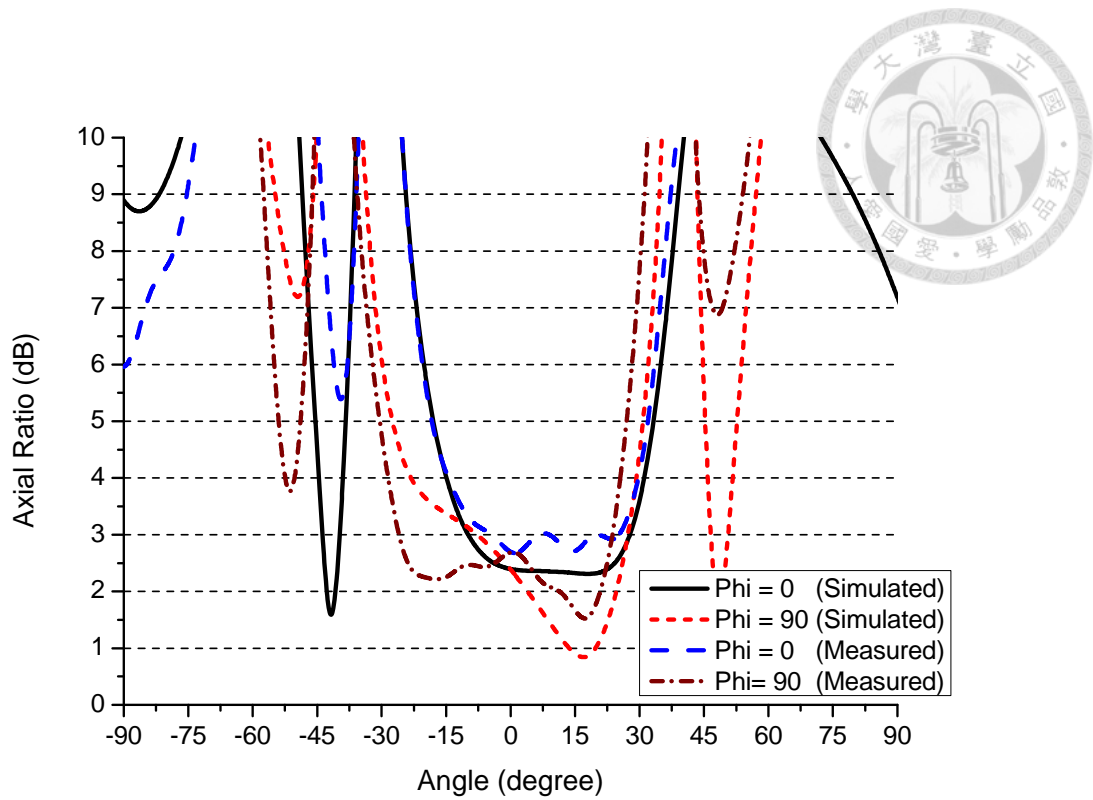
Fig. 3.32 Simulated and measured axial ratio beam width with taper lines (Port 1 excited)
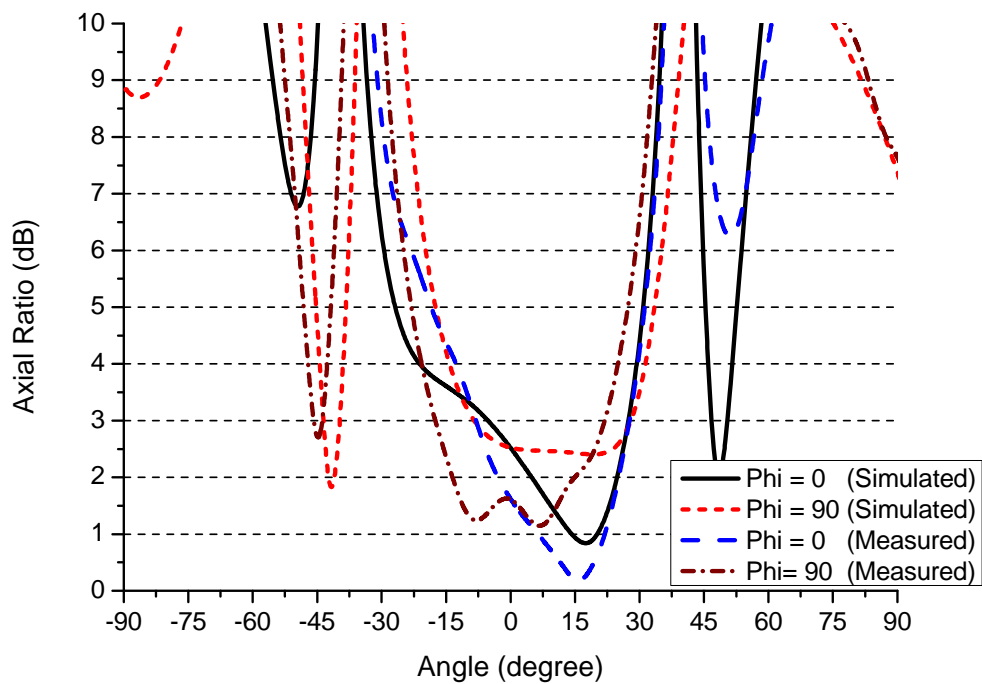

Fig. 3.33 Simulated and measured axial ratio beam width with taper lines (Port 2 excited)

Chapter 4 Dual-Feed Oversize Patch Antenna with Dual Circular Polarization at 61 GHz ISM band
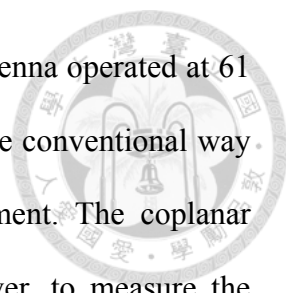
In this chapter, the dual circularly polarized oversize patch antenna operated at 61 GHz is based on quarter wave transformer technique which is viewed in section 3.1. The oversize antenna is designed to cover the 61 GHz ISM band with dual circular polarization and high gain at broadside direction.

4.1 Antenna Design

The prototype of the proposed antenna is operated at 61 GHz shown in Fig. 4.1. The dielectric substrate is Rogers RT/duroid5880 with dielectric constant $\epsilon_r = 2.2$, loss tangent $\tan\delta = 0.0009$ and thickness $h = 0.127$ mm. The feeding microstrip lines are designed to match the 50-Ω connectors. All design parameters are listed in Table 4.1, where the definition of parameters is the same as the 5.8 GHz ISM band version in section 3.1.

4.2 Simulation and Measurement Results

The simulated and measured S-parameters of 61 GHz ISM band antenna are shown in Fig. 4.2. In 5.8 GHz version, the transmission coefficient bandwidth is larger than reflection coefficient bandwidth. In 61 GHz version, the reflection coefficient bandwidth is larger than transmission coefficient. The S-parameter bandwidth is restricted by $|S_{21}|$ bandwidth. The simulated isolation bandwidth is around 1.08% (60.9~61.56 GHz) which just covers 61 GHz ISM band (61~61.5 GHz). The in-band

isolation between two ports is better than 15 dB. To measure the antenna operated at 61 GHz, the measurement environment must be designed carefully. One conventional way to measure a millimeter wave antenna is the on-wafer measurement. The coplanar microwave probes are exploited to measure S-parameters. However, to measure the radiation patterns of the antenna, the jig is needed to hold the antenna and fix the connectors. Since the substrate thickness is very thin, the fixture can avoid the substrate distorted. From the reasons above, the 1.85mm connectors is used to measure the S-parameters and radiation patterns. Besides, in order to prevent the 1.85mm connectors touching each other, the ground size is chosen larger than 20mm. The measured S-parameters shown in Fig. 4.2 are better than simulated results. The measured $|S_{11}|$ and $|S_{22}|$ are not identical. It is because port 1 is connected to vector network analyzer while port 2 is connected through cable line. The measured impedance bandwidth covers 59 GHz to 62.5 GHz. In this bandwidth, the isolation is better than 20dB.

In Fig. 4.3 and Fig.4.4, the simulated realized gain at dip point of isolation is shown. These simulated results do not consider the jig effect that conforms to the antenna characteristic. The RT/5880 dielectric constant is closer to air which lead to large side lobe level. Similarly, the perturbation from the microstrip lines results to the radiation patterns are not symmetry along z-axis. Moreover, the radiation patterns are degraded since the ground size with respect to guided wave is much larger than previous. The simulated peak realized gain is up to 7.5 dBic as shown in Fig 4.5. In Fig. 4.6, the efficiency is up to 75% in band. The axial ratio bandwidth is shown in Fig. 4.7. In addition, the axial ratio beam width at center frequency is plotted in Fig. 4.8 and Fig. 4.9. The simulated axial ratio beam width of port 1 is from -9° to 11° at X-Z plane and from -7° to 7.6° at Y-Z plane.

As mention above, the jig is needed to hold the antenna and fix the connectors to

measure the radiation patterns of the antenna. The jig has two conductor walls beside the antenna that are set to the connectors. This restriction results in pattern distortion. The simulated realized gain with conductive jig and measured realized gain are shown in Fig. 4.10 and Fig 4.11. The maximum value of simulated and measured pattern tilts a little angles due to the conductive jig effect. The simulated peak realized gain at dip point of isolation is about 9.5 dBic while the measured peak realized gain at dip point of isolation is about 5.5 dBic. It is because that the simulated results do not consider the connecter effect, manufacturing error and measurement deviation.

4.3   Conclusion

The proposed oversize dual circularly polarized patch antenna has been applied in 61 GHz ISM band. The characteristics of antenna such as high gain at broadside direction and port-to-port isolation are similar to previous design in Chapter 3. In millimeter wave, the physical dimension of antenna is extremely small. Comparing with the conventional antenna, the proposed oversize antenna is much easier to match the input impedance satisfying minimum line width restrictions. Furthermore, the error tolerance in fabrication can be increased due to the enlarged size. This design concept is full of promise in millimeter wave applications.
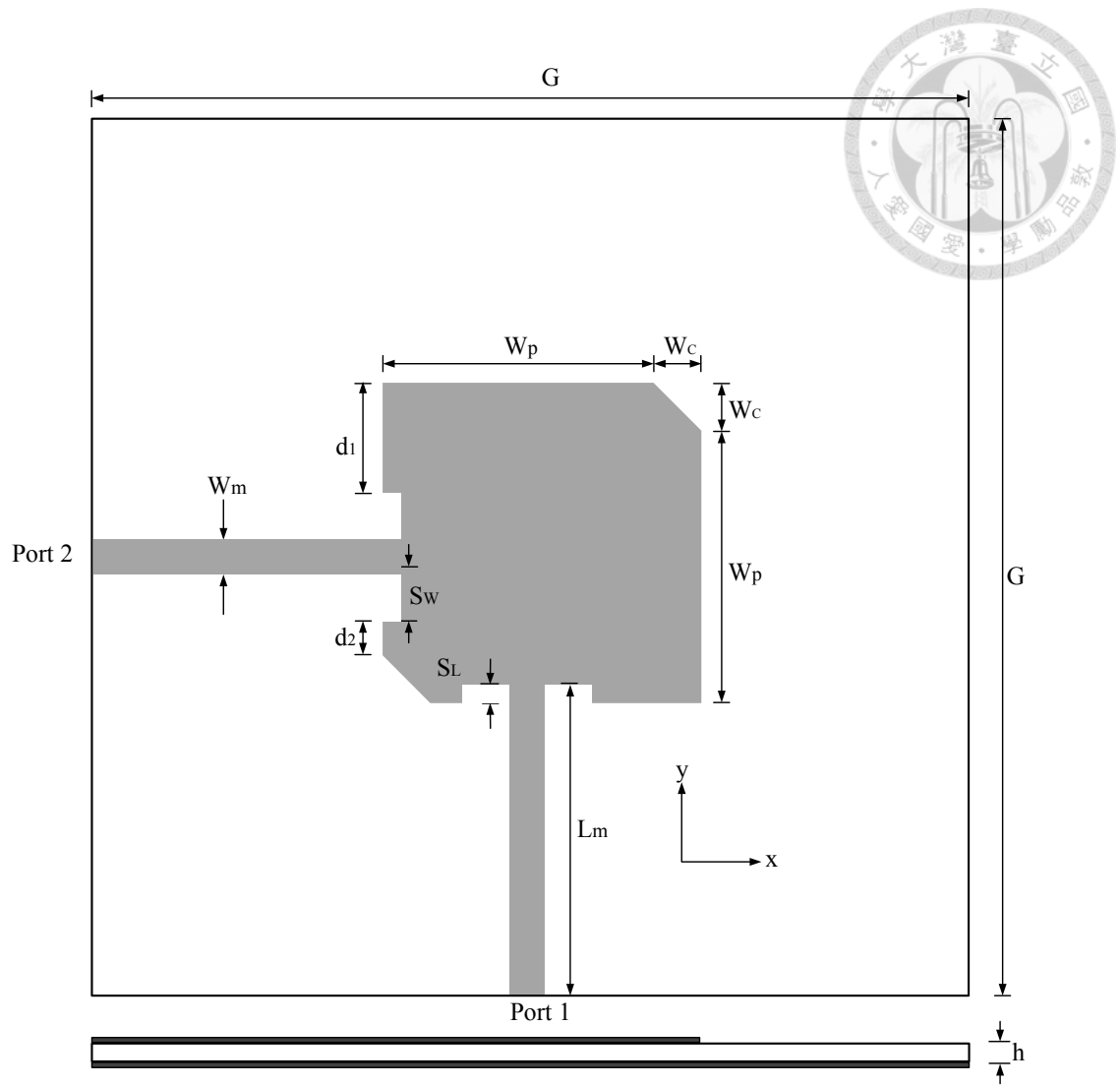
Fig. 4.1 A prototype of oversize antenna operating at 61 GHz

Design Parameters (Unit : mm)			
G	h	W_p	W_c
20	0.127	4.18	0.6
d_1	d_2	S_L	S_W
1.64	1.04	0.15	0.6
L_m	W_m		
10.05	0.3		

Table 4.1 Design parameters of the oversize patch antenna operating at 61 GHz
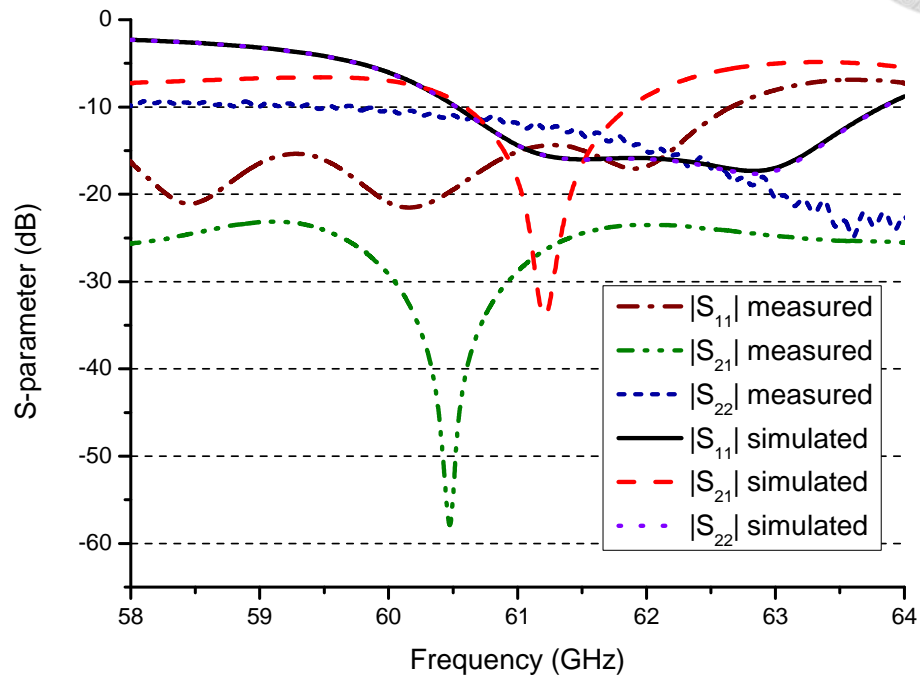
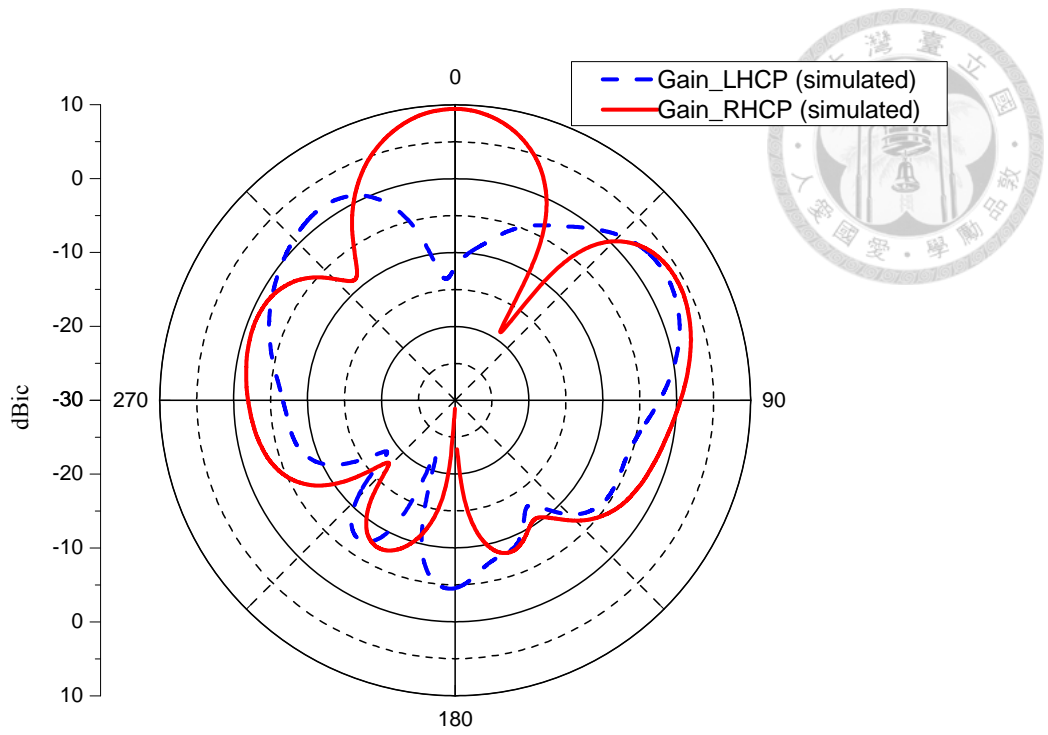Fig. 4.2 Simulated and measured S-parameters of 61 GHz ISM band antenna

(a) X-Z plane
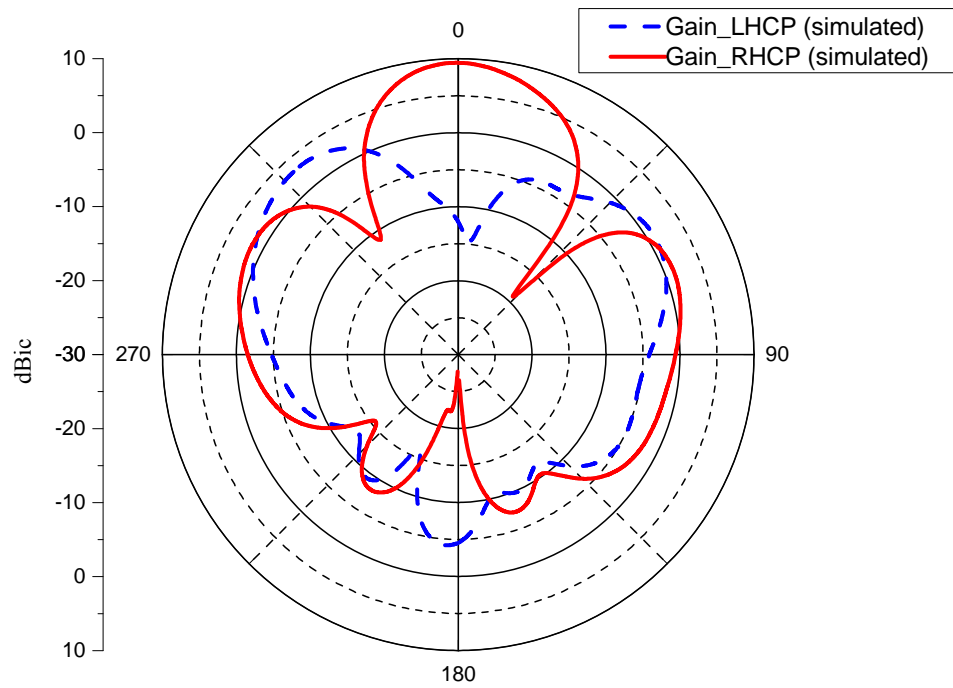
(b) Y-Z plane

Fig. 4.3 Simulated realized gain without fixing jig (Port 1 excited)

(a) X-Z plane

(b) Y-Z plane

Fig. 4.4 Simulated realized gain without fixing jig (Port 2 excited)

61

Fig. 4.5 Simulated peak realized gain
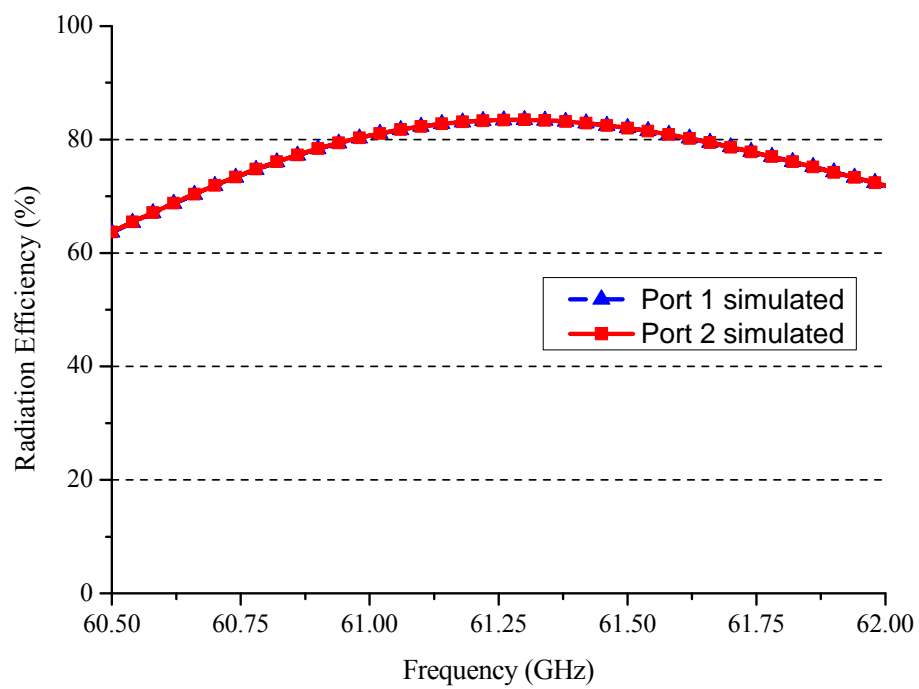
Fig. 4.6 Simulated radiation efficiency

62

Fig. 4.7 Simulated axial ratio for 61 GHz band

Fig. 4.8 Simulated and measured axial ratio beam width (Port 1 excited)

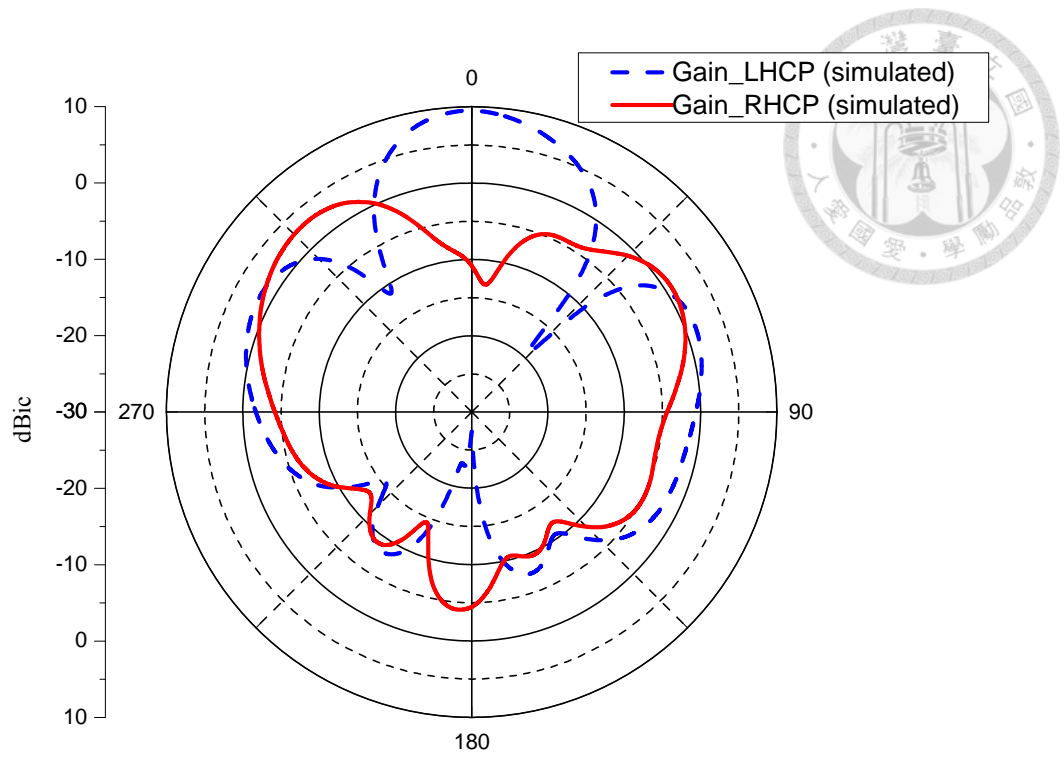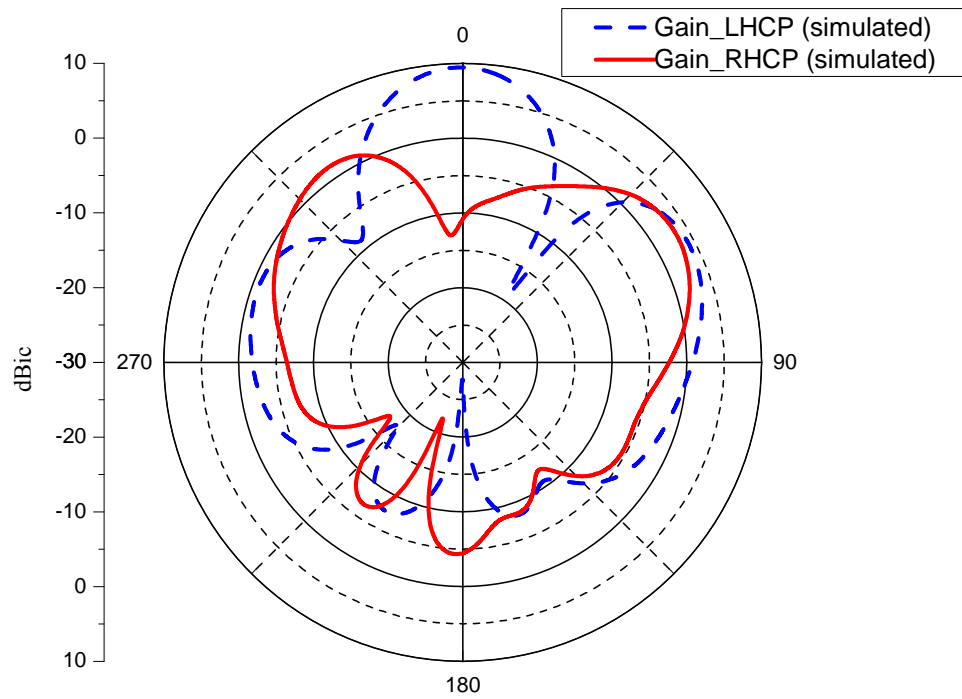Fig. 4.9 Simulated and measured axial ratio beam width (Port 2 excited)

(a) X-Z plane

(b)   Y-Z plane

Fig. 4.10 Simulated and measured realized gain with fixing jig (Port 1 excited)

(a) X-Z plane

(b) Y-Z plane

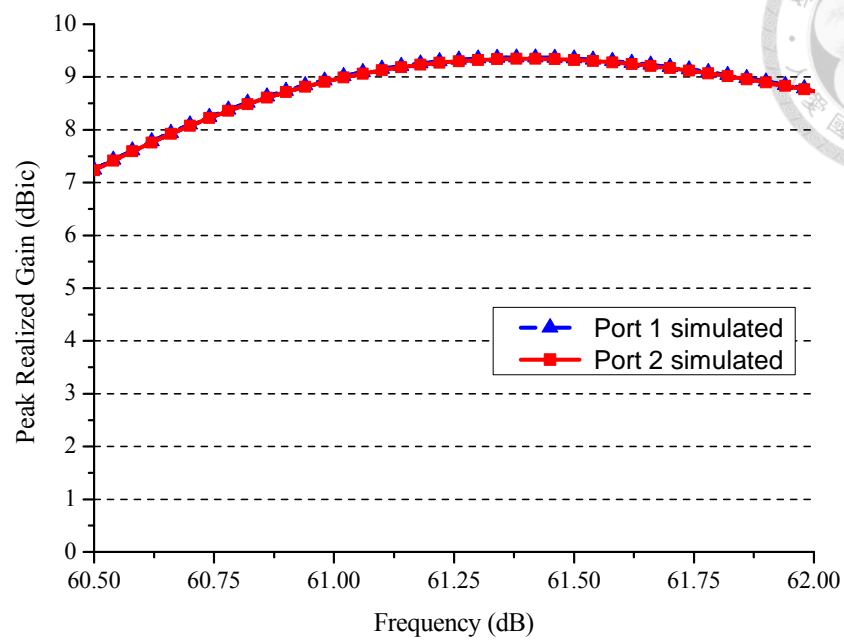Fig. 4.11 Simulated and measured realized gain with fixing jig (Port 2 excited)

66

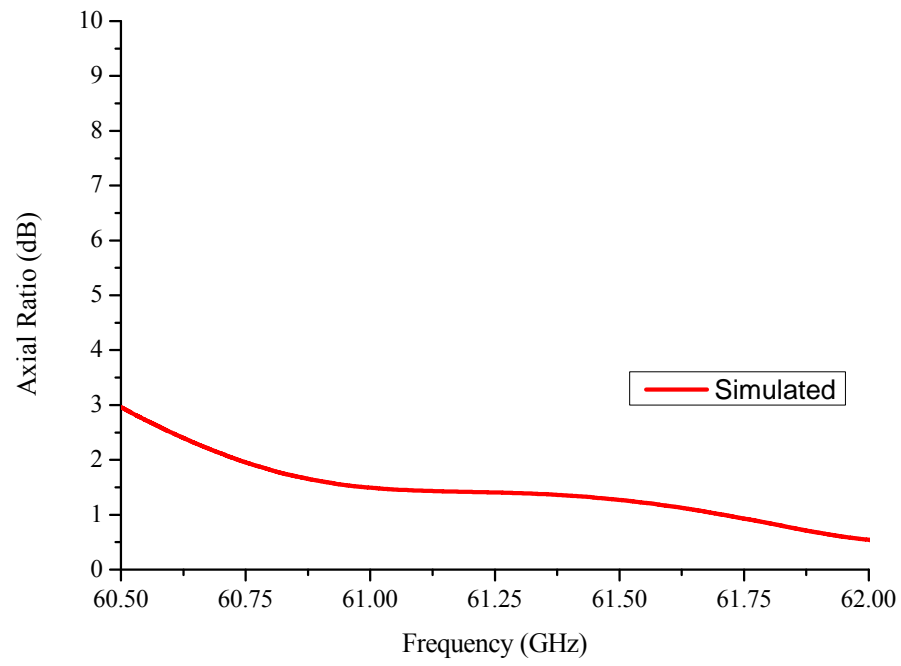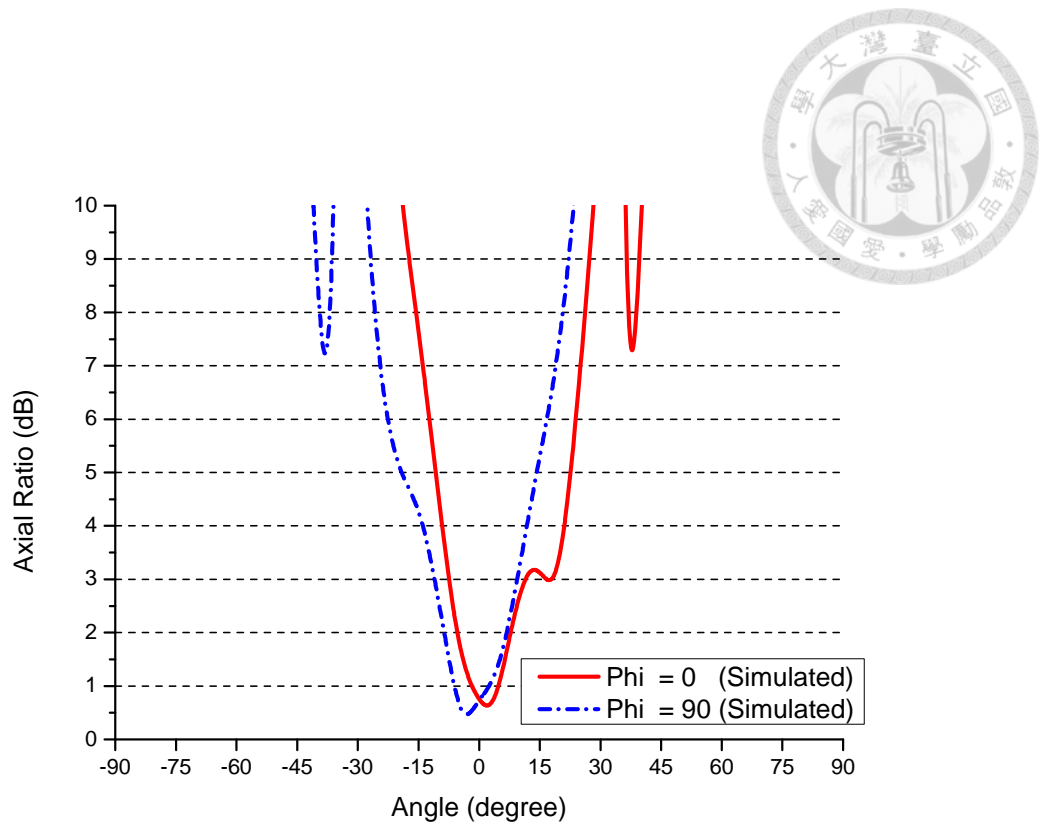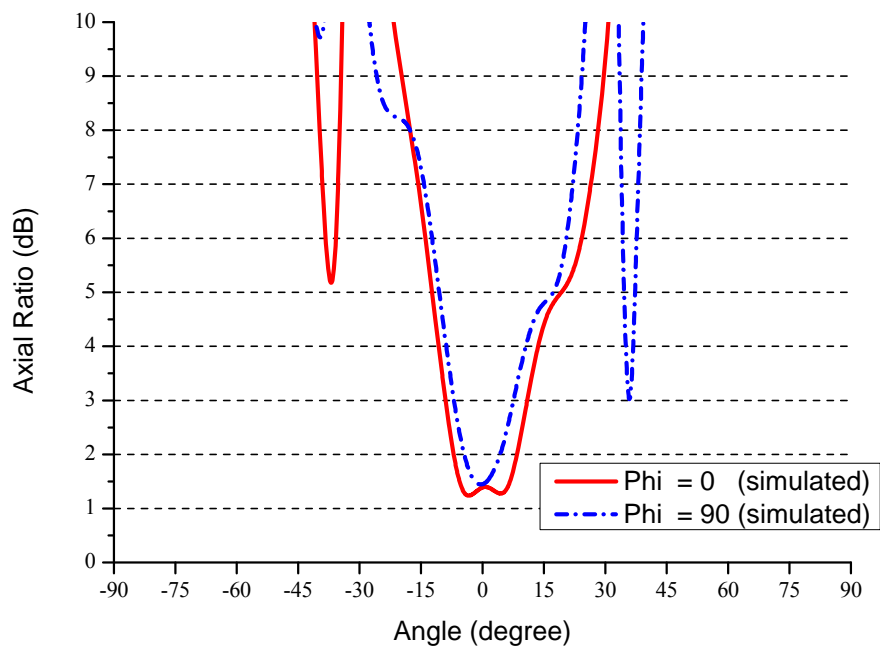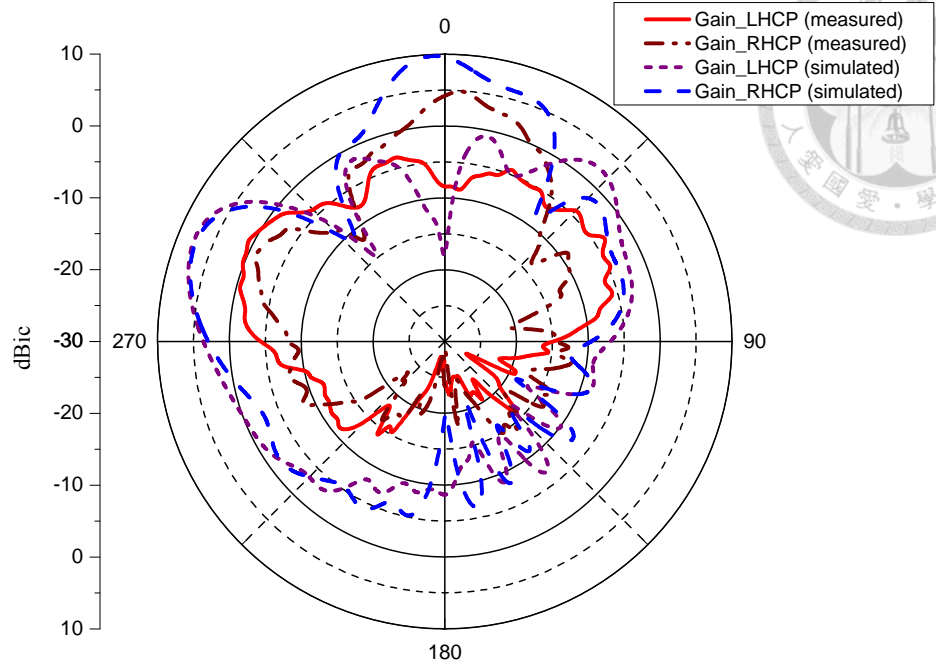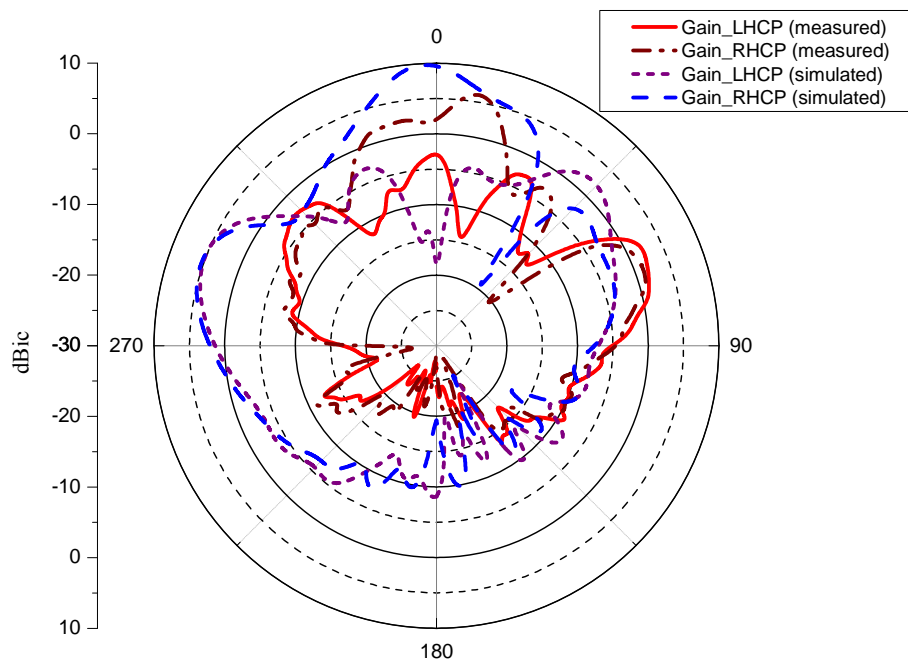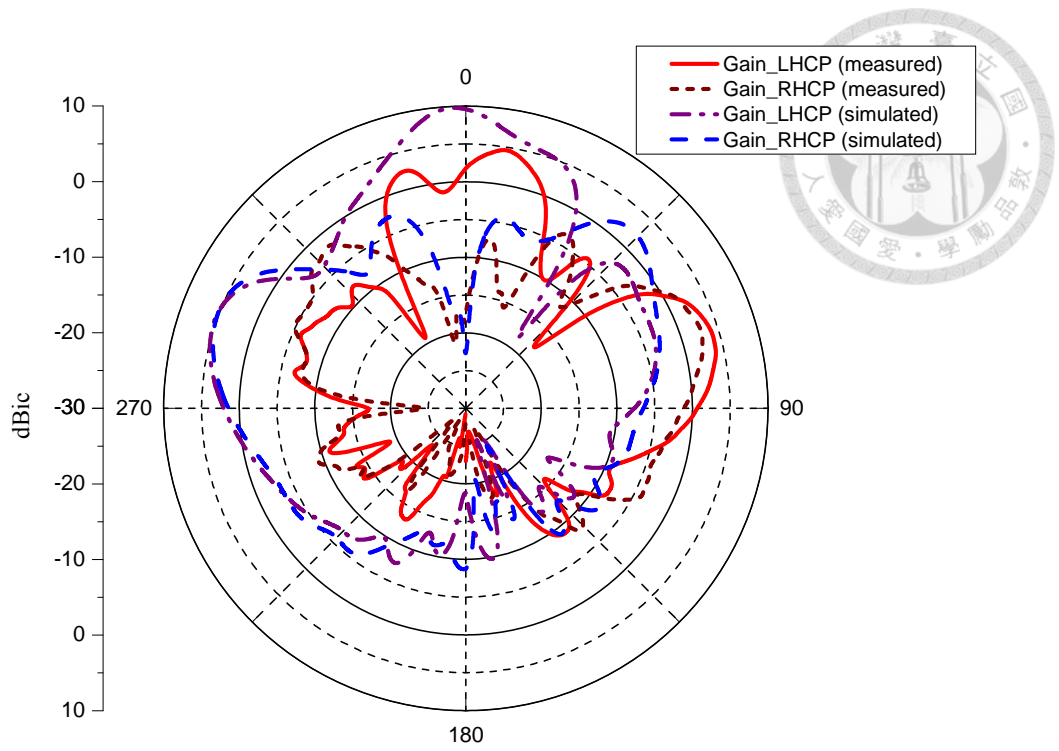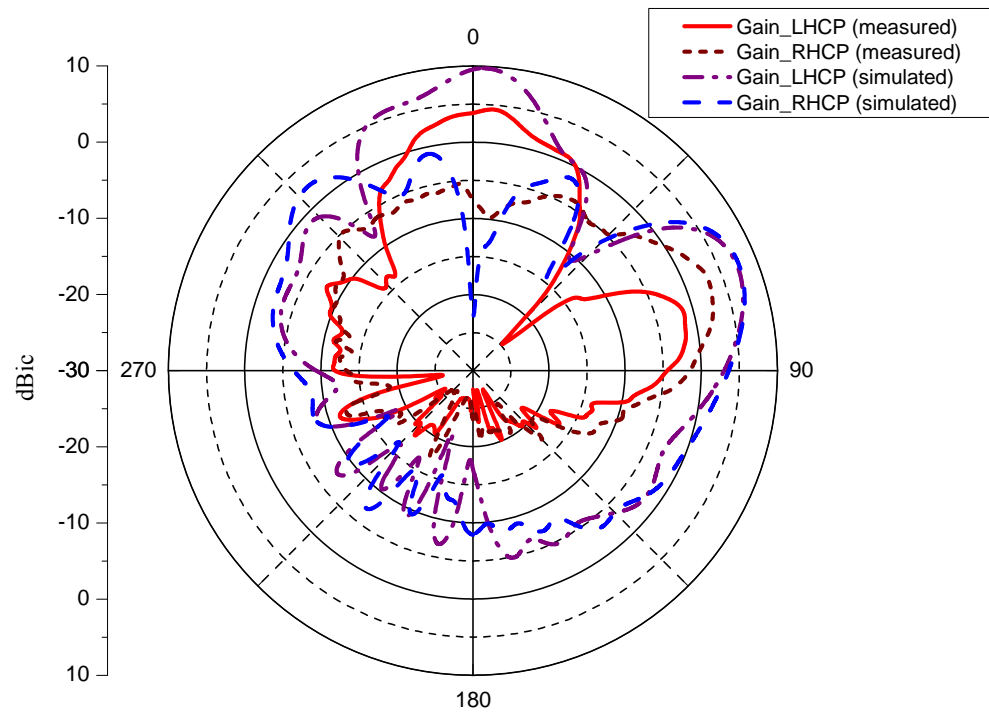# Chapter 5   Conclusion and Future Works

5.1   Conclusion

In this thesis, a dual-feed circularly polarized oversize patch antenna for polarization diversity applications has been proposed. This antenna has a simple structure in a single layer. Dual circular polarization has been achieved by exciting the patch by two orthogonal ports individually. By using TM_{30} mode, the oversize antenna has high gain characteristic at broadside direction without using any array elements. Comparing to the conventional circularly polarized patch antenna, the oversize antenna has more than one electric field null, so that the isolation between the two ports can be achieved by choosing proper feeding positions. However, the impedance bandwidth is limited by the antenna itself, which is proved by changing matching transformers. Nevertheless, the impedance bandwidth and axial ratio bandwidth of the experimentally proposed antenna can cover the 61 GHz ISM band (61 ~ 61.5 GHz). This design has been verified at 5.8 GHz ISM band. Satisfactory agreement between simulation and measurement has been achieved.

The oversize antenna is very useful in the millimeter-wave applications. At 61 GHz, the physical dimension of the antenna are so small that they result in fabrication difficulty. Also, the conventional edge-fed patch antenna has a problem of mismatch due to technological limitations. Moreover, the patch antenna may not be the main radiator since the microstrip feeding line is as large as the conventional antenna. These problems can be solved by using the proposed oversize antenna. In the oversize design, the impedance matching is easier than that of the conventional patch, that is to say, the enlarged antenna does not need any complicated matching networks. Last but not least,

the manufacturing error tolerances of the fabrication can be relaxed by using the oversize design.

5.2   Future Work

As mention in Section 3.1, the isolation can be enhanced by finding the electric field null. The isolation between the two ports is above 15 dB that is not good enough. Some isolation techniques could be used to enhance the isolation. However, the axial ratio bandwidth may be worse than before if the isolation techniques influence the current distribution on microstrip patch.

Another issue is that the radiation pattern is degraded in 61 GHz version antenna due to the surface wave and feeding lines effect. By using electromagnetic band gap structure, the surface wave can suppressed in effect.
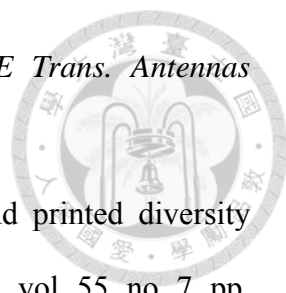
REFERENCE
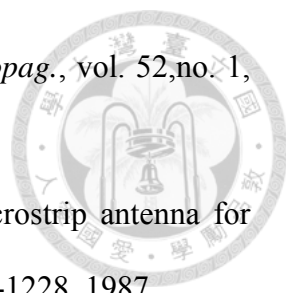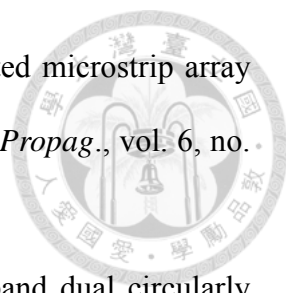
[1] S. Gao, Q. Luo, and F. Zhu, *Circularly polarized antennas*, 1st ed., West Sussex: Wiley, 2014.

[2] S. Mann, G. Vinci, S. Lindner, S. Linz, F. Barbon, R. Weigel, and A. Koelpin, "61 GHz six-port radar frontend for high accuracy range detection applications," in Proc. *Antennas and Propag. in Wireless Commun.*, Sept. 2013, pp. 818-821.

[3] S. Scherr, S. Ayhan, H.Gulan, M. Pauli, and T. Zwick, "61 GHz ISM band FMCW radar for applications requiring high accuracy, " in Proc. *Asia-Pacific Microw. Conf.*, Sendai, Japan, Nov. 2014, pp. 1118-1120.

[4] A. Stelzer, C. Diskus, K. Lubke, and H. Thim, "A microwave position sensor with submillimeter accuracy, " *IEEE Transactions on Microwave Theory and Techniques*, vol.47, no. 12, pp. 2612-2624, Dec.1999.

[5] M. PourMousavi, M. Wojnowski, S. Roehr, G. Sommer, R. Weigel, "The impact of shape and size of air cavity on extended hemispherical lens characterization for wireless applications at 61 GHz," in Proc. *European Antennas and Propag. Conf.*, Gothenburg, Sweden, April 2013, pp. 3295-3298.

[6] M. Umehira, T. Sasame, and H. Sawada, "An orthogonal polarization based MIMO transmission for advanced 60 GHz WLAN," in Proc. *IEEE Vehicular Technology Conf.*, Yokohama, Japan, May 2012, pp.1-5.

[7] H. K. Pan, "Dual-polarized Mm-wave phased array antenna for multi-Gb/s 60 GHz communication," in Proc. *IEEE AP-S Int. Symp.*,Spokane, USA, July 2012, pp. 3279-3282.

[8] C. A. Balanis, *Antenna Theory – Analysis and Design*, 3rd ed., New York: Wiley,

2005.

[9]   R. Bancroft, *Microstrip and Printed Antenna Design*, 2nd ed., SciTech Publishing, 2009.

[10]   C. K. Yang, "A 60 GHz patch antenna with dual-feed for polarization diversity applications," M.S. thesis, National Taiwan University, Taiwan, 2013.

[11]   Y. J. Ren and K. Chang, "A new class of harmonic components for millimeter-wave applications," *Int. Journal of RF and Microwave Comp. Aid Eng.*, pp 63-67, 2008.

[12]   E. Okon and C. Turner, "High order mode planar resonators for mm-wave applications" in Proc. *IEEE Symp. High Perform Electron Devices Microwave Optoelectronic Applications*, London, UK, Nov. 1999, pp. 307-311.

[13]   D. Wang, H. Wong, K. B. Ng, and C. H. Chan, "Wideband shorted higher-order mode millimeter-wave patch antenna," in Proc. *Int. Symp. Antennas Propag.*, Chicago, USA, July 2012, pp. 1-2.

[14]   Y. H. Kung, "60-GHz Dual-feed oversized patch antenna for polarization diversity applications," M.S. thesis, National Taiwan University, Taiwan, 2014.

[15]   B. Allen, R. Brito, M. Doher, and H. Aghvami, "Performance comparison of spatial diversity array topologies in an OFDM based wireless LAN," *IEEE Trans. Consumer Electronics*, vol. 50, no. 2, pp. 420-428, May 2004.

[16]   E. G. Larsson, "On the combination of spatial diversity and multiuser diversity," *IEEE Commun. Letter*, vol. 8, no. 8, pp. 517-519, Aug. 2004.

[17]   T. A. Tsifitsis, H. G. Sandalidis, G. K. Karagiannidis, and M. Uysal, "Optical wireless links with spatial diversity over strong atmospheric turbulence channels," *IEEE Trans. Wireless Commun.*, vol. 8, no. 2, pp. 951-957, Feb. 2009.

[18]   H. T. Chattha, Y. Huang, S. J. Boyes, and X. Zhu, "Polarization and pattern

diversity-based dual-feed planar inverted-F Antenna," *IEEE Trans. Antennas Propag.*, vol. 60, no. 3, pp. 1532-1539, Mar. 2012.

[19] Y. Ding, Z. Du, K. Gong, and Z. Feng, "A novel dual-band printed diversity antenna for mobile terminals," *IEEE Trans. Antennas Propag.*, vol. 55, no. 7, pp. 2028-2096, Jul. 2007.

[20] M. Gallo, E. A D., M. F B., M. Bozzetti, J. M. M.-G-P., and L. J. –L., "A broadband pattern diversity annular slot antenna," *IEEE Trans. Antennas Propag.*, vol. 60, no. 3, pp.1593-1600, Mar. 2012.

[21] S. H. Chen, J.-S. Row, K. L. Wong, "Reconfigurable square-ring patch antenna with pattern diversity," *IEEE Trans. Antennas Propag.*, vol. 55, no. 2, pp.472-475, Feb. 2007.

[22] Y. Dong, and T. Itoh, "Planar ultra-wideband antennas in Ku- and K-band for pattern or polarization diversity applications," *IEEE Trans. Antennas Propag.*, vol. 60, no. 6, pp. 2886-2895, June 2012.

[23] L. J. Du Toit and J. H. Cloete, "Dual polarized linear microstrip patch array," in Proc. *IEEE AP-S Int. Symp.*, Blacksburg, USA, 1987, pp. 810-813.

[24] M. J. Cryan and P. S. Hall, "Integrated active antenna with simultaneous transmit-receive operation," *Electron. Lett*, vol. 32, no. 4, pp. 286-287, Feb. 1996.

[25] S. S. Zhong, X. X. Yang, S. C. Gao, and J. H. Cui, "Corner-fed microstrip antenna element and arrays for dual polarization operation," *IEEE Trans. Antennas Propag.*, vol. 50, no. 10, pp. 1473-1480, Oct. 2002.

[26] K. S. Min, S. H. Park, D. C. Kim, and H. Arai, "Microstrip patch antenna with dual resonance and dual polarization," in Proc, *Asia Pacific Microwave Conf.*, 1999, vol. 1, pp. 158-161.

[27] H. Wong, K. L. Lau and K. M. Luk, "Design of dual-polarized L-probe patch

antenna arrays with high isolation," *IEEE Tran. Antennas Propag.*, vol. 52,no. 1, pp. 45-52, Jan. 2004.

[28] A. Adrain and D. H. Schaubert, "Dual aperture-coupled microstrip antenna for dual or circular polarization," *Electron. Lett.*, vol. 23, pp. 1226-1228, 1987.

[29] S. Gao, L. W. Li, M. S. Leong, and T. S. Yeo, "A broad-band dual-polarized microstrip patch antenna with aperture coupling," *IEEE Tran. Antennas Propag.*, vol. 51, no. 4, April 2003.

[30] K. L. Wong, H. C. Tung, and T. W. Chiou, "Broadband dual-polarized aperture-coupled patch antennas with modified H-shaped coupling slots," *IEEE Tran. Antennas Propag.*, vol. 50, no. 2, Feb. 2002.

[31] T. W. Chiou and K. L. Wong, "Broad-band dual-polarized single microstrip patch antenna with high isolation and low cross polarization," *IEEE Tran. Antennas Propag.*, vol. 50, no. 3, Feb. 2002.

[32] D. G. Kurup, A. Rydberg, and M. Himid, "Compact microstrip-T coupled patch antenna for dual polarization and active antenna applications," *Electron. Lett.*, vo. 38, no. 21, pp.1240-1241, Oct. 2002.

[33] F. Ferrero, C. Luxey, R. Staraj, G. Jacquemod, M. Yedlin, and V. Fusco, "Theory and design of a tunable quasi-lumped quadrature coupler," *Microwave Opt. Technol. Lett.*, vol. 51, no. 5, pp. 2219-2222, Sep. 2009.

[34] F. Ferrero, C. Luxey, R. Staraj, G. Jacquemod, M. Yedlin, and V. Fusco, "A novel quad-polarization agile patch antenna" *IEEE Trans. Antennas Propag.*, vol. 57, no. 5, pp. 1563-1567, May 2009.

[35] W. Zhu, S. Xiao, R. Yuan, and M. Tang, "Broadband and dual circularly polarized patch antenna with H-shaped aperture," in Proc, *Antennas and Propag. (ISAP), 2014 Int. Symp. on*, Kaohsiung, Taiwan, Dec. 2014, vol. 1, pp. 167-168.

[36] Y. Ushijima, E. Nishyama, M. Aikawa, "Single-layer integrated microstrip array antenna for dual circular polarization," *IET Microw. Antennas Propag.*, vol. 6, no. 8, pp. 962-968, 2011.

[37] C. Zhang, X. Liang, X. Bai, J. Geng, and R. Jin, "A broadband dual circularly polarized patch antenna with wide beamwidth," *IEEE Antennas Propag. Lett.*, vol.13, pp. 1457-1460, 2014.

[38] G. L. Wu, W. Mu, G. Zhao, and Y. C. Jiao, "A novel design of dual circularly polarized antenna fed by L-strip," *Progress In Electromagnetics Research*, vol. 79, pp. 39-46. 2008.

[39] A. Narbudowicz, X. Bao, and M. Ammann, "Dual circularly-polarized patch antenna using even and odd feed-line modes," *IEEE Trans. Antennas Propag.*, vol. 61, no. 9, pp. 4828-4831, Sep. 2013.

[40] F. Yang and Y. Rahmat-Samii, "A reconfigurable patch antenna using switchable slots for circular polarization diversity," *IEEE Microwave Wireless Compon. Lett.*, vol. 12, no. 3, pp. 96-98, Mar. 2002.

[41] T. Fukusako, N. Kitamura, and N. Mita, "Circularly polarized reconfigurable patch antenna using Y-branched feed circuit," in Proc. *IEEE AP-S Int. Symp.*, July 2005, pp. 597-600.

[42] S. Gao, Q. Luo, and F. Zhu, *Circularly Polarized Antennas*, 1st ed., New York: Wiley, 2014.

[43] J. S. Hong, *Microstrip Filter for RF/Microwave Applications*, 2nd ed., New York: Wiley.